RESEARCH ARTICLE

Key Points:
- Radiocarbon activity of NW Pacific is reconstructed with benthic-planktonic data
- Shape of radiocarbon activity profiles is not sensitive to Delta-R used
- LGM deep North Pacific depleted in C-14 but BA profile shape similar to modern

Supporting Information:
- Readme
- Animation S1
- Figure S1
- Table S1
- Table S2

Correspondence to:
M. S. Cook,
mea.s.cook@williams.edu

Radiocarbon profiles of the NW Pacific from the LGM and deglaciation: Evaluating ventilation metrics and the effect of uncertain surface reservoir ages

Mea S. Cook[1] and Lloyd D. Keigwin[2]

[1]Geosciences Department, Williams College, Williamstown, Massachusetts, USA, [2]Geology and Geophysics Department, Woods Hole Oceanographic Institution, Woods Hole, Massachusetts, USA

Abstract During the last deglaciation, the ventilation of the subarctic Pacific is hypothesized to have changed dramatically, including the rejuvenation of a poorly ventilated abyssal water mass that filled the deep ocean, and fluctuations in the strength of North Pacific intermediate and deep water formation at millennial timescales. Foraminiferal radiocarbon reconstructions of past ventilation changes in the Pacific are valuable but are hampered by poor carbonate preservation, low sediment accumulation rates, bias from bioturbation, and poorly constrained past surface reservoir age. In this study, we present paired benthic-planktonic radiocarbon measurements from the Okhotsk Sea and Emperor Seamounts. We take advantage of large contemporaneous peaks in benthic abundances from the last glacial maximum, Bolling-Allerod (BA), and early Holocene to produce time slices of radiocarbon from 1 to 4 km water depth. We explore the impact of uncertain surface reservoir age and evaluate several approaches to quantifying past ocean radiocarbon distribution using our NW Pacific data and a compilation of published data from the North Pacific. Both the calendar age and the absolute value of an ocean radiocarbon estimate depend on the assumed surface reservoir age. But for a time slice from a small geographical area with radiocarbon-independent stratigraphic correlation between cores, the shape of a water column profile is independent of surface reservoir age. The NW Pacific profiles are similar in shape to the compilation profiles for the entire North Pacific, which suggests that deglacial surface reservoir age changes across the N Pacific did not diverge dramatically across the areas sampled. The Last Glacial Maximum (LGM) profile >2 km spans a wide range of values, ranging from values similar to today to lower than today. However, by the BA the profile has a similar shape to today. Ultimately, local surface reservoir ages, end-member water mass composition, and mixing ratios must each be constrained before a radiocarbon activity reconstruction can be used to confidently infer ventilation changes.

1. Introduction

Radiocarbon estimates of the past ocean are valuable because unlike passive nutrient-proxy tracers, radiocarbon has the potential to trace both the distribution of water masses and their transport. Radiocarbon reconstructions of the past ocean are from radiocarbon measurements in marine carbonates: benthic and planktonic foraminifera, colonial corals, solitary corals, and bivalves. A well-known problem with estimates that rely on calibrated (calendar) ages from planktonic foraminifera is that most studies assume that the offset between the radiocarbon age of the local surface water and the atmosphere (the "surface reservoir age") has been constant through time. If this offset was different in the past, the estimated calendar age of the planktonic foraminifera will be biased. Since the sample age is used to correct the measured benthic $\Delta^{14}C$ for the decay since it grew, a biased surface reservoir age results in an incorrect estimate of the past ocean $\Delta^{14}C$.

According to model simulations, variations in deep ocean circulation or atmospheric ^{14}C production rate can change the surface reservoir age by hundreds of years on centennial to millennial timescales [*Butzin et al.*, 2005; *Franke et al.*, 2008; *Ritz et al.*, 2008]. Therefore, with varying ocean circulation and cosmogenic nuclide flux through the latest Pleistocene, we can expect that surface reservoir ages may have changed globally in the past, and not necessarily uniformly. This potentially complicates the dating of key rapid climate events and evaluation of the relative timing of change between locations. In addition, unaccounted for changes in surface reservoir age of hundreds of years can introduce as large a signal into a $\Delta^{14}C$ reconstruction as the changes associated with ocean circulation. Therefore, precise interpretation of foraminiferal radiocarbon
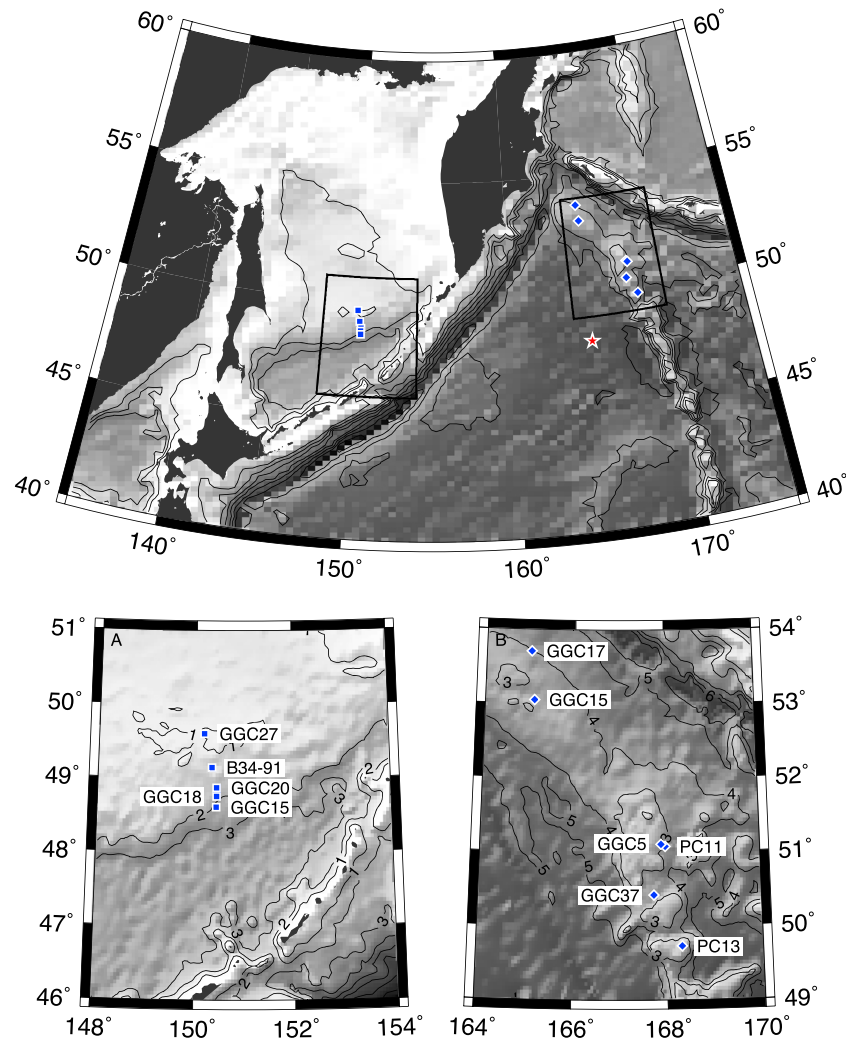
Figure 1. Location of cores from the Okhotsk Sea (squares) and Emperor Seamounts (diamonds). Bathymetry from *Smith and Sandwell* [1997]. Contour interval is 1 km. The location of WOCE Line P13 Station 23 (1992) is marked by the red star.

reconstructions requires an independent age model. Unfortunately, these estimates are rare [e.g., *Sikes et al.*, 2000; *Sarnthein et al.*, 2007; *Marchitto et al.*, 2007; *Ikehara et al.*, 2011].

Comparison of published deep-ocean radiocarbon data from the Last Glacial Maximum (LGM) ocean is hampered by the wide variety of approaches of inferring past ocean circulation with radiocarbon. The approaches include using benthic-planktonic foraminiferal radiocarbon age differences [*Keigwin*, 2004], using benthic-atmosphere $\Delta^{14}C$ differences [*Robinson et al.*, 2005], and using benthic-atmosphere radiocarbon age differences [e.g., *Sarnthein et al.*, 2007; *Skinner et al.*, 2010]. There is the projection correction [*Adkins and Boyle*, 1997] relative to either the atmosphere [*Galbraith et al.*, 2007] or the surface ocean [*Skinner and Shackleton*, 2004] to account for the varying atmospheric $\Delta^{14}C$ through time. The transit-time distribution, equilibration-time distribution (TTD-ETD) method accounts for diffusive mixing in the ocean interior [*DeVries and Primeau*, 2010]. Each of these approaches accounts for different processes and makes a different set of assumptions, resulting in quantities that are difficult to compare to each other and to the modern ocean.

As the largest ocean basin, the Pacific plays a large role in the heat and salt budget of the ocean, and the partitioning of carbon dioxide between the atmosphere and seawater, and is a major focus of radiocarbon-based paleo-circulation studies. Benthic foraminiferal carbon and oxygen stable isotopes [*Herguera et al.*, 1992; *Keigwin*, 1998, 2002; *Matsumoto et al.*, 2002] suggest that during the LGM, there was a boundary at 2 km between a well-ventilated water mass above and a poorly ventilated water mass of Southern Ocean origin below

Table 1. Sediment Coring and Hydrographic Station Locations

Cruise	Core	Depth (m)	Latitude (°N)	Longitude (°E)
		Okhotsk Sea		
NES 25-1	GGC27	995	49.601	150.180
Volcanolog	B34-91	1227	49.142	150.337
NES 25-1	GGC20	1510	48.874	150.432
NES 25-1	GGC18	1700	48.752	150.431
NES 25-1	GGC15	1980	48.608	150.428
		Emperor Seamounts		
RNDB	PC13	2329	49.725	168.312
RNDB	GGC5	2804	51.112	167.895
RNDB	PC11	3225	51.073	168.975
VINO 19-4	GGC37	3300	50.420	167.732
RNDB	GGC15	3700	51.050	168.097
VINO 19-4	GGC17	3960	53.707	165.013
		Hydrographic Station		
WOCE P13	23		47.990	165.002

(see review by *Adkins* [2013]). During the deglaciation, it is hypothesized that there was an antiphase relationship between the strength of meridional overturning in the North Atlantic and North Pacific [*Mikolajewicz et al.,* 1997], where a deep water mass formed in the subarctic Pacific during Heinrich Stadial 1 (HS1) [*Okazaki et al.,* 2010; *Jaccard and Galbraith*, 2013; *Rae et al.,* 2014] and possibly the Younger Dryas [*Okazaki et al.,* 2014]. Nearly all of the radiocarbon reconstructions of the North Pacific circulation from the Last Glacial Maximum (LGM) and deglaciation assume a constant, preindustral local surface reservoir age [e.g., *Duplessy et al.,* 1988; *Ahagon et al.,* 2003; *Galbraith et al.,* 2007; *Okazaki et al.,* 2010; *Lund et al.,* 2011].

In this paper we present a depth transection of radiocarbon data from the northwest Pacific from the Emperor Seamounts and the Okhotsk Sea (Figure 1). The Emperor and Okhotsk cores were previously used to construct profiles of stable isotopes during the Last Glacial Maximum and Holocene [*Keigwin*, 1998]. This regional study provides coherent profiles of water column radiocarbon, which are all from peaks in abundance of benthic foraminifera. This allows us to overcome the effects of low abundance, poor preservation and low sediment accumulation rates that frequently plague attempts for high-quality radiocarbon data from the glacial and deglacial Pacific [*Oxburgh and Broecker*, 1993; *Mekik*, 2014]. In addition, some of the peaks in *Uvigerina* abundance are coeval in multiple cores, allowing us to make robust time slices of the water column, and estimate the relative enrichment and depletion of radiocarbon with depth. We use these data to compare several methods of inferring past ocean circulation with radiocarbon and the effects of varying local surface reservoir ages on interpreting radiocarbon data. Finally, we compile benthic-planktonic radiocarbon data from the literature from cores across the North Pacific and evaluate how well it constrains the radiocarbon structure of that basin from the last deglaciation.

2. Methods

2.1. Micropaleontology

The Emperor Seamounts cores were collected during Roundabout Leg 6 on R/V *Thomas Washington* in 1988, and R/V *Akademic Aleksandr Vinogradov* 19-4 in 1991; the Okhotsk Sea cores were collected from R/V *Akademic Aleksandr Nesmeyanov* 25-1 in 1993 (Table 1). For the micropaleontology work, we took 1 cm or 2 cm thick samples from the cores, dried them at 50°C, and then disaggregated and washed the samples over 63 μm sieves. We counted the number of the two *Uvigerina* species present, *Uvigerina peregrina* and *Uvigerina senticosa*, in the >150 μm size fraction and calculated absolute abundance as number per gram dry sediment (Figure 2). The benthic $\delta^{18}O$ stratigraphies in Figure 2 are from *Keigwin* [1998]. Gaps in the isotope stratigraphies are due to samples with insufficient foraminifera for analysis.

We picked benthic (*U. peregrina* and *U. senticosa*) and planktonic (*Neogloboquadrina pachyderma* (sinistral), *Globigerina bulloides*) foraminifera for accelerator mass spectrometry radiocarbon dating at peaks of absolute abundance. Radiocarbon analyses were performed at National Ocean Sciences Accelerator Mass Spectrometry
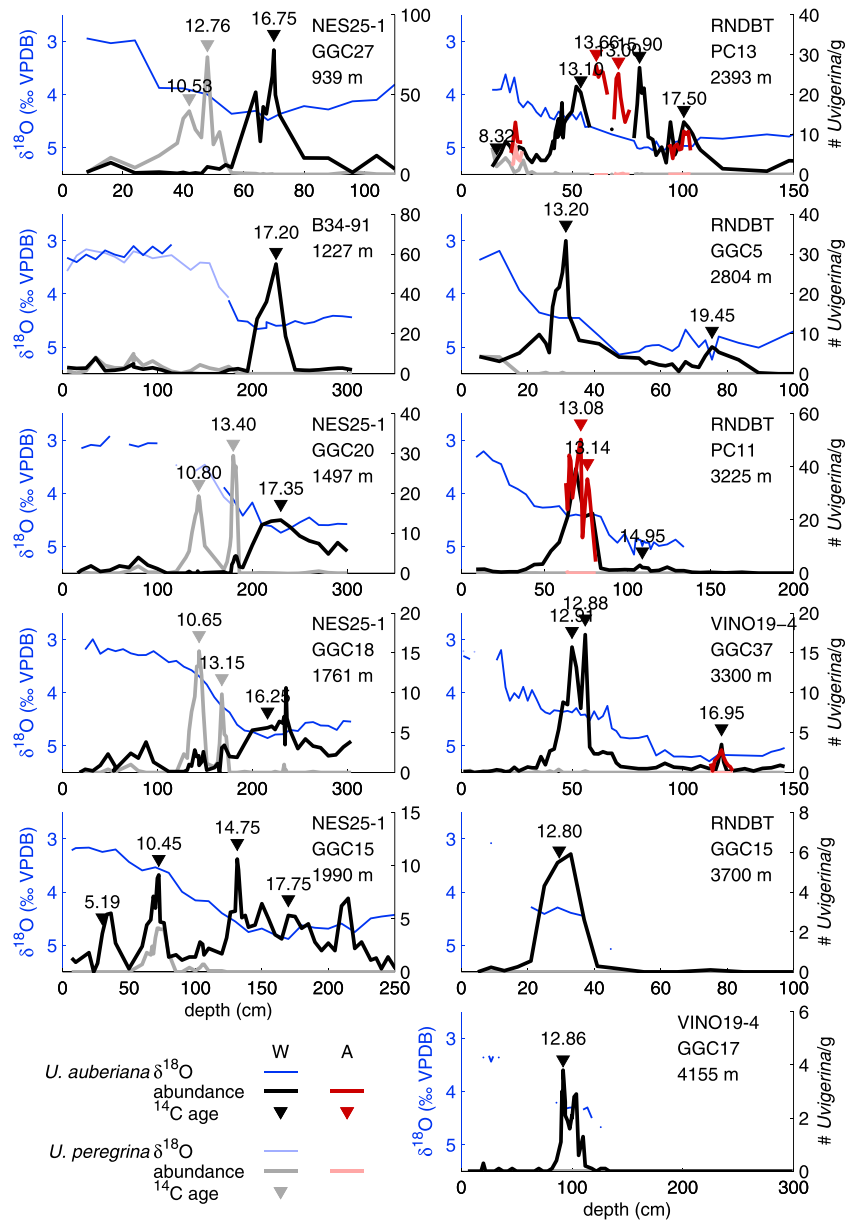
Figure 2. The $\delta^{18}O$ of *U. senticosa* (dark blue) and *U. peregrina* (pale blue), with the absolute abundance of *U. senticosa* (black) and *U. peregrina* (grey). Gaps in the isotope stratigraphies are due to samples with insufficient foraminifera for analysis. Triangles mark the samples with paired *Uvigerina* and planktonic radiocarbon dates. Abundance and radiocarbon data from the archive half of the sediment core are in red/pink. The triangles are annotated with the uncalibrated, uncorrected planktonic radiocarbon ages in ^{14}C kyr.

Facility in Woods Hole, Massachusetts. Table 2 includes our 41 new radiocarbon measurements and 17 previously published radiocarbon measurements [*Keigwin*, 1998, 2002; *Brunelle et al.*, 2010]. Some of the previously published data are not identical to what is reported in those publications due to the application of a reference blank correction.

2.2. Local Surface Reservoir Age

The offset in radiocarbon age between the atmosphere surface ocean is the surface reservoir age [*Bard*, 1988]. We estimated the local, preindustrial anomaly (ΔR) from the global reservoir correction to be 390 ± 100 years, meaning that the surface reservoir age ($R + \Delta R$) was 790 ± 100 years. This estimate is the weighted mean of

Table 2. Radiocarbon Measurements From the Okhotsk Sea and Emperor Seamounts

Core Name	Water Depth (m)	Depth (cm)	Planktonic Species	Age ±1σ (y)	Depth (cm)	Benthic Species	Age ±1σ (years)	Peak #
NES25-1 GGC27	995	41.5–42.5	*G. bulloides*	10,530 ± 60	41.5–42.5	*U. peregrina*	11,650 ± 85	1
		47.0–49.0	*G. bulloides*	12,760 ± 55	47.0–49.0	*U. peregrina*	13,900 ± 90	2
		69.0–71.0	*N. pachyderma* (s.)	16,750 ± 200[a]	69.0–71.0	*U. senticosa*	18,200 ± 95[a]	3
B34-91	1227	224.0–226.0	*N. pachyderma* (s.)	17,200 ± 80[a]	225?	*U. senticosa*	18,650 ± 110[a]	3
NES25-1 GGC20	1510	143.0–144.0	*G. bulloides*	10,800 ± 45	143.0–144.0	*U. peregrina*	11,750 ± 60	1
		179.0–181.0	*G. bulloides*	13,400 ± 50	179.0–181.0	*U. peregrina*	14,450 ± 85	2
		229.0–231.0	*N. pachyderma* (s.)	17,350 ± 100[a]	230?	*U. senticosa*	18,700 ± 140[a]	3
NES25-1 GGC18	1700	143.0–145.0	*G. bulloides*	10,650 ± 50	143.0–145.0	*U. peregrina*	11,600 ± 55	1
		167.0–169.0	*G. bulloides*	13,150 ± 65	167.0–169.0	*U. peregrina*	14,100 ± 50	2
		215.0–217.0	*N. pachyderma* (s.)	16,250 ± 120[a]	213.0–215.0	*U. senticosa*	17,800 ± 140[a]	
NES25-1 GGC15	1980	29.0–31.0	*N. pachyderma* (s.)	5,190 ± 35[b]	29.0–31.0	*U. senticosa*	6,840 ± 50	
		72.0–73.0	Mixed species	10,450 ± 50	72.0–73.0	*U. senticosa*	11,350 ± 70	1
		131.0–132.0	Mixed species	14,750 ± 70	131.0–132.0	*U. senticosa*	15,850 ± 90	
		169.0–171.0	*N. pachyderma* (s.)	17,750 ± 100[b]	169.0–171.0	*U. senticosa*	19,350 ± 130[b]	3
RNDB PC13	2329	15.0–17.0	*G. bulloides*	8,320 ± 35[c]	15.0–17.0	*U. peregrina*	7,690 ± 45	
		53.0–55.0	*G. bulloides*	13,100 ± 70[c]	53.0–55.0	*U. senticosa*	14,800 ± 65	2
		60.5–61.5	Mixed species	13,660 ± 90[c]	60.5–61.5	*U. senticosa*	16,000 ± 85	
		79.0–82.0	*N. pachyderma* (s.)	15,900 ± 60[c]	79.0–82.0	*U. senticosa*	17,350 ± 90	
		100.0–101.0	*N. pachyderma* (s.)	17,500 ± 110[c]	100.0–101.0	*U. senticosa*	20,100 ± 160	3
RNDB GGC5	2804	31.0–32.0	*G. bulloides*	13,200 ± 75	31.0–32.0	*U. senticosa*	14,900 ± 55	2
		75.0–77.0	Mixed species	19,450 ± 120	75.0–77.0?	*U. senticosa*	21,900 ± 160	
RNDB PC11	3225	71.5–72.5[e]	*G. bulloides*	13,080 ± 60	71.5–72.5	*U. senticosa*	14,400 ± 85	2
		75.5–76.5[e]	*G. bulloides*	13,140 ± 70	75.5–76.5	*U. senticosa*	14,200 ± 80	2
		108.0–109.0	*N. pachyderma* (s.)	14,950 ± 85	108.0–112.0	*U. senticosa*	16,650 ± 110	
VINO19-4 GGC37	3300	49.0–51.0	*N. pachyderma* (s.)	12,910 ± 95[b]	49.0–51.0	*U. peregrina*	13,280 ± 115	2
		55.0–57.0	*N. pachyderma* (s.)	12,880 ± 115[b]	55.0–57.0	*U. peregrina*	13,260 ± 110	2
		117.0–118.0[d]	*N. pachyderma* (s.)	16,950 ± 65	113.0–114.0[d]	*U. senticosa*	17,500 ± 100	3
RNDB GGC15	3700	29.0–30.0	*G. bulloides*	12,800 ± 50	29.0–30.0	*U. senticosa*	13,850 ± 110	2
VINO19-4 GGC17	3950	90.0–95.0	*N. pachyderma* (s.)	12,860 ± 35	90.0–95.0	*U. senticosa*	13,750 ± 80	2

[a]From *Keigwin* [2002].
[b]From *Keigwin* [1998].
[c]From *Brunelle et al.* [2010].
[d]Sample from both working and archive halves of the core.
[e]Sample from archive half of the core.

nine North Pacific locations with estimates of ΔR from the Calib Database [*Reimer and Reimer*, 2001]: Vancouver Island (330 ± 80 years), Middleton Island (340 ± 50 years), Kodiak Island (320 ± 50 years), Graham Island (265 ± 80 years) [*McNeely*, 2006], Pavlov Harbor, AK, (242 ± 50 years) [*Robinson and Thompson*, 1981], Kunashir Island (380 ± 110 years) [*Kuzmin et al.*, 2001], Shikotan Island (490 ± 40 years), Sakhalin Island (400 ± 30 years) [*Yoneda et al.*, 2007], and the Okhotsk Sea (578 ± 50 years) [*Kuzmin et al.*, 2007]. In locations with more than one estimate, these were averaged to produce a single age per location. We excluded Calib Database [*Reimer and Reimer*, 2001] reservoir age estimates from inlets, fjords, or close to land, since they do not represent the open ocean.

There are a handful of estimates of North Pacific surface reservoir age during the LGM and deglaciation. Deglacial estimates include 700 years from associated wood and marine carbonates from SW British Columbia [*Kovanen and Easterbrook*, 2002], and 600–700 years from marine tephrochronology off SE of Japan during the Bolling-Allerod [*Ohkushi et al.*, 2007; *Ikehara et al.*, 2011]. Using radiocarbon plateau "tuning," LGM to deglacial estimates of ΔR are ~1400 years off Vancouver Island [*Cosma et al.*, 2008] and 800–3200 years in the subarctic Pacific [*Sarnthein et al.*, 2007]. In this latter study, the wide range in radiocarbon ventilation age estimates from just three sediment cores clearly points to the need for more studies that evaluate the ΔR changes across the North Pacific during the LGM and deglaciation.

To account for the possibility that surface reservoir age may have changed by hundreds of years in the past, we consider values for local ΔR ranging from 0 to 1200 ^{14}C years in increments of 100 years (corresponding to a total surface reservoir age of 400 to 1600 ^{14}C years). For each of the subsequent calculations of past ocean radiocarbon (described in the next section), we perform the calculation for each value of ΔR. The error

bar of a single calculation includes only the uncertainty in the radiocarbon measurement and radiocarbon calibration curve, and utilizes a single value of ΔR. Comparison of calculations using a range of values of ΔR illustrates the variation due to ΔR alone.

2.3. Analyzing Foraminiferal Radiocarbon Data

In the present study, we focus on simply reconstructing the distribution of radiocarbon in the past ocean ($\Delta^{14}C_0$). In analyzing the new NW Pacific data set, we will assess several ways of contextualizing radiocarbon estimates from the past deep ocean in order to evaluate how different it was from the preindustrial ocean (t_{B-P}, t_{B-Atm}, $\Delta^{14}C_{0-Atm}$, $\Delta^{14}C_{0,adj}$, see Table 3). We will then compare these metrics to a commonly used method of estimating a timescale of ocean ventilation, the projection age (t_{Proj}) [*Adkins and Boyle*, 1997].

The measured radiocarbon age ($\Delta^{14}C$ converted into equivalent ^{14}C years) of a water parcel in the ocean is not the same as the radiocarbon ventilation age (the timescale of transport as recorded by the decay of radiocarbon). This is because the $\Delta^{14}C$ of a parcel is affected not only by the timescale of transport but also the initial $\Delta^{14}C$ of the constituent water masses of the parcel and the mixing ratio of the constituents [*Matsumoto*, 2007; *Broecker et al.* 1991; *Stuiver et al.* 1983]. Ocean circulation can affect $\Delta^{14}C$ of a water parcel in the deep ocean in several ways. An increase in $\Delta^{14}C$ could result if the transit time of a constituent water mass decreases, the fraction contribution of a higher-$\Delta^{14}C$ water masses increases, or the $\Delta^{14}C$ of an end-member water mass increases. In the last case, there are multiple mechanisms that can have this effect, for example, changes in the hydrography of the water mass formation area and consequent modification of the water mass being formed or a change in atmospheric $\Delta^{14}C$. The number of source areas assumed to contribute to a water parcel in the deep ocean also has a significant effect on the estimated radiocarbon ventilation age [*Gebbie and Huybers*, 2012].

Even if the end-members and water mass mixing are well constrained, a radiocarbon ventilation age is not an intrinsic property of a water mass. Tracer age estimates vary depending on the tracer used and its radioactive decay constant [*Waugh et al.*, 2003; *Wunsch and Heimbach*, 2008]. This is because with advective and diffusive transport there is no single pathway by which water travels from the source area to the interior ocean. Instead, there are multiple pathways, resulting in a distribution of ages [*Haine and Hall*, 2002; *DeVries and Primeau*, 2010]. The "mean age" corrects for the transit-time distribution and is tracer independent.

As we gain a fuller understanding of the characteristics of glacial and deglacial water mass end-members from radiocarbon and passive tracers [*Robinson and van de Flierdt*, 2009; *Burke and Robinson*, 2012; *Skinner et al.*, 2010; *Skinner*, 2013, 2014], and the evolution of the distribution of water masses in the ocean basins [*Matsumoto et al.*, 2002; *Curry and Oppo*, 2005; *Lynch-Stieglitz et al.*, 2007], we will be able to refine our understanding of the relationship between radiocarbon distribution and ocean ventilation. In the future, this may resolve some of the perplexing enigmas from radiocarbon-based studies on where carbon dioxide was sequestered in the deep ocean during the LGM [*Broecker et al.*, 2004; *Broecker and Clark*, 2010; *Hain et al.*, 2010; *Lund et al.*, 2011; *Lund*, 2013] and how the pathways and timing of the repartitioning of carbon dioxide between the deep ocean and atmosphere proceeded during the deglaciation [*Marchitto et al.*, 2007; *Bryan et al.*, 2010; *De Pol-Holz et al.*, 2010; *Lund et al.*, 2011].

In the remainder of this section, we will briefly summarize each of the radiocarbon metrics discussed in this paper, including how it is calculated, the assumptions behind the calculation, and how to compare it with the preindustrial world. See Table 3 and Figure 3 for summaries of these methods.

2.3.1. The Benthic-Planktonic Age Difference (t_{B-P})

The simple difference between the radiocarbon ages of benthic and planktonic samples is t_{B-P} (Figure 3c). Because benthic and planktonic foraminifera that lived at the same time have the same true age, the difference in their radiocarbon ages reflect differences in the radiocarbon age of the water they grew in, which is related to circulation [*Broecker et al.*, 1984]. Radiocarbon ages are calculated using the Libby decay constant, $\lambda_L = 8033^{-1}$ yr^{-1}, rather than the true decay constant, $\lambda_C = 8266^{-1}$ yr^{-1} [*Stuiver and Polach*, 1977]. So we compare t_{B-P} data to a reference curve, the $\Delta^{14}C$ from nearby World Ocean Circulation Experiment (WOCE) Line P13 station 23 (600 m and deeper), converted to radiocarbon age (using λ_L), minus the radiocarbon age of local surface water ($R + \Delta R$). The greatest advantage of t_{B-P} is its simplicity. However, it must be interpreted with caution, keeping in mind that local reservoir age affects the planktonic radiocarbon age.

Table 3. Methods for Estimating Past Ocean Radiocarbon[a]

Name	Unit	Baseline of comparison	Modern reference curve	Notes	Source
(1) Benthic-planktonic age difference (t_{B-P})	^{14}C y	Local surface water	Radiocarbon age profile minus local surface water age using the Libby decay constant	Simplest method.	Broecker et al. [1988]
(2) Benthic-atmosphere age difference (t_{B-Atm})	^{14}C y	Contemporary atmosphere	Radiocarbon age profile using the Libby decay constant	Equivalent to $\Delta^{14}C_{0,adj}$ and $\Delta^{14}C_{0-Atm}$ with unit conversion. Comparable across all time periods.	Sarnthein et al. [2007]; Skinner et al. [2010]
(3a) Projection age (t_{Proj})	cal y[b]	Past atmosphere	Radiocarbon age profile using the Cambridge decay constant	Accounts for changing $\Delta^{14}C_{Atm}$ through time propagated into interior ocean.	Adkins and Boyle [1997]
(3b) Modified projection age (t_{Proj2})	cal y	Past atmosphere	Radiocarbon age profile using the Cambridge decay constant	Accounts for changing $\Delta^{14}C_{Atm}$ propagated into interior ocean. Modified from original t_{Proj} to project to average global surface ocean $\Delta^{14}C$, rather than projecting to the atmosphere then applying local surface reservoir correction.	Skinner and Shackleton [2004]
(1) Transit-time distribution – equilibration-time distribution age ($t_{TTD-ETD}$)	cal y	Past atmosphere	Radiocarbon age profile using the Cambridge decay constant	Accounts for diffusive mixing and changing $\Delta^{14}C_{Atm}$ through time.	DeVries and Primeau [2010]
(5) Initial benthic $\Delta^{14}C$ ($\Delta^{14}C_0$)	‰	Pre-industrial atmosphere	Modern $\Delta^{14}C$ profile corrected for higher past $\Delta^{14}C$ everywhere	Estimate of the benthic $\Delta^{14}C$ at the time it grew. Can be used for calculating radiocarbon budgets.	Adkins and Boyle [1997]
(6) $\Delta^{14}C_0$ anomaly from the contemporary atmosphere ($\Delta^{14}C_{0-Atm}$)	‰	Contemporary atmosphere	Modern $\Delta^{14}C$ profile corrected for higher past $\Delta^{14}C$ everywhere minus the contemporary $\Delta^{14}C_{Atm}$	Equivalent to t_{B-Atm} with unit conversion. Not directly comparable to other time periods since $\Delta^{14}C$ gradients depend on total radiocarbon in the atmosphere-ocean system.	Various
(7) Initial benthic $\Delta^{14}C$ corrected to a world with $\Delta^{14}C_{Atm}=0$ ($\Delta^{14}C_{0,adj}$)	‰	Contemporary atmosphere	Modern $\Delta^{14}C$ profile	Equivalent to t_{B-Atm} with unit conversion. Comparable across all time periods.	This study

[a]None of these methods account for changing mixing ratios of source water masses or changes in source water composition, and all are affected an incorrect surface reservoir age.
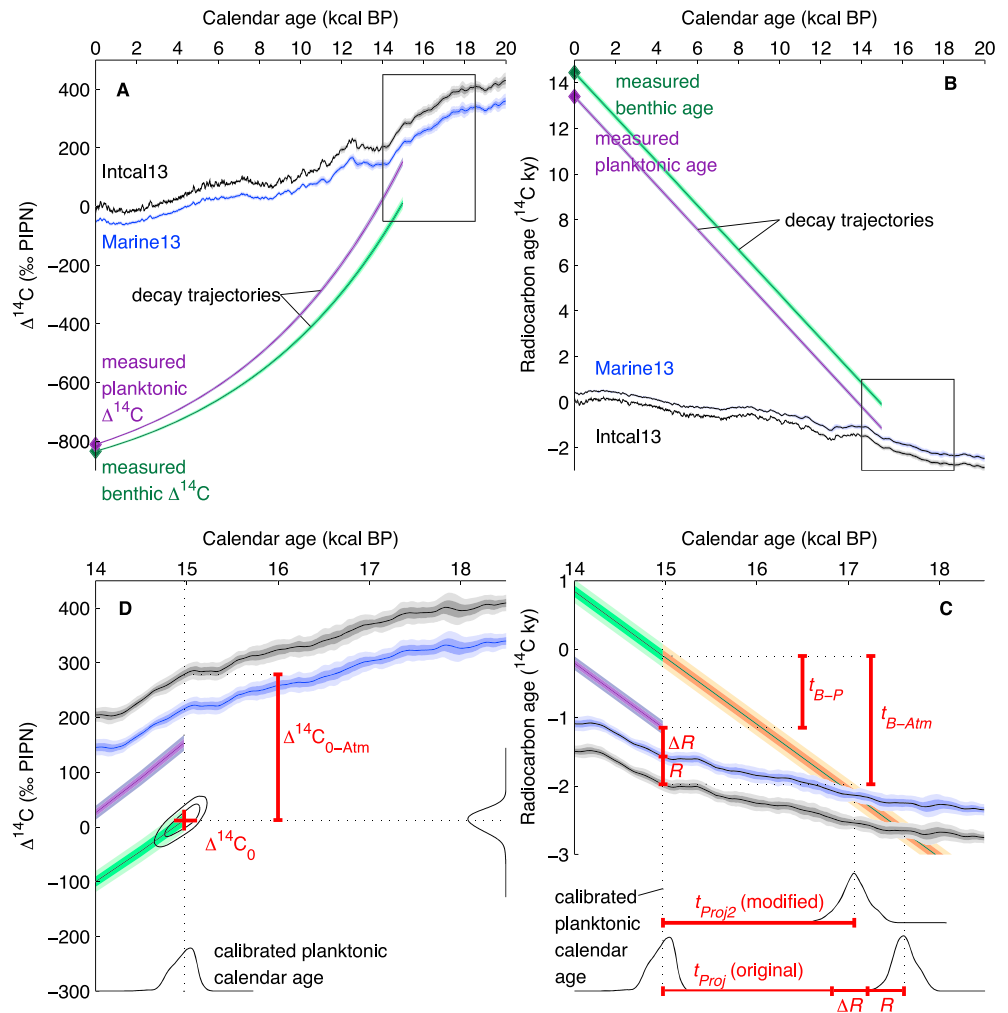[b]The unit cal y means calendar year.

Figure 3. Schematic diagram illustrating radiocarbon data analysis methods. (a and b) Measured benthic and planktonic radiocarbon ages/Δ^{14}C are in green and purple diamonds, and the lines show the decay trajectories through time. The Intcal13 and Marine13 [*Reimer et al.*, 2013] data sets are in black and blue, respectively. The light and dark shaded areas show the 1σ and 2σ uncertainty in the radiocarbon measurement. The boxes in Figures 3a and 3b correspond to the domains in Figures 3d and 3c, respectively. (c) The calibrated planktonic calendar age is the intersection of the mean surface ocean and the planktonic decay trajectory minus the surface reservoir age ($R + \Delta R$). The benthic-planktonic difference in radiocarbon years is t_{B-P}. The difference in radiocarbon age of the benthic sample and contemporary atmosphere, converted into permil units, is Δ^{14}C$_{0,adj}$. In orange is the decay trajectory of the hypothetical water mass that the benthic foraminifera grew in, for calculation of the "projection age" [*Adkins and Boyle*, 1997]. Thin black lines show the probability distribution functions of the calendar age, the intersection of the water mass decay trajectory (orange) with the surface ocean and atmosphere. The original projection age is the difference between the calendar age and the intersection of the water mass decay trajectory with the atmosphere, minus the local surface reservoir age ($R + \Delta R$). The modified projection age used in this study is the difference between the calendar age and the intersection of the water mass decay trajectory with the mean surface ocean. (d) The Δ^{14}C$_0$ is the initial Δ^{14}C of the benthic sample at the time it grew and is the intersection of the benthic decay trajectory and the calendar age of the sample. The Δ^{14}C$_{0-Atm}$ is the difference between the Δ^{14}C$_0$ and the contemporary atmosphere. Thin black contours show the shape of the joint probability distribution functions of Δ^{14}C$_0$. The thick red lines show the 1σ uncertainties in the x and y directions. Thin black lines show the probability distribution functions of the calendar age, Δ^{14}C$_0$ and Δ^{14}C$_{0-Atm}$.

2.3.2. The Initial Benthic Δ^{14}C (Δ^{14}C$_0$)

The Δ^{14}C of the benthic foraminiferal tests at the time they grew (Δ^{14}C$_0$) is an estimate of the Δ^{14}C of the water they grew in (Figure 3d). We derive this quantity by correcting the measured Δ^{14}C of the benthic foraminifera for the decay that had taken place since the foraminifera were alive to get the Δ^{14}C when the sample grew [*Adkins and Boyle*, 1997]. In equation (1), the measured Δ^{14}C is Δ^{14}C$_A$ and the Δ^{14}C when the

sample grew is $\Delta^{14}C_B$, where y is the calibrated calendar age of the sample from the planktonic foraminifera radiocarbon measurement

$$\Delta^{14}C_A = 1000\left[\left(\frac{\Delta^{14}C_B}{1000} + 1\right)e^{\lambda_C y} - 1\right]. \tag{1}$$

We use λ_C (the true decay constant) here since y is in calendar years. The virtue of $\Delta^{14}C_0$ is that it estimates the actual radiocarbon activity of the ocean in the past and can be used in assessing radiocarbon budgets. This quantity is useful for studying the time evolution of radiocarbon in the ocean with changing ocean circulation and global radiocarbon inventory. The greatest uncertainty in estimating $\Delta^{14}C_0$ is the surface reservoir age assumed when calculating the calendar age from the planktonic radiocarbon measurement, since the $\Delta^{14}C_0$ is an exponential function of calendar age.

A disadvantage of $\Delta^{14}C_0$ is that it cannot be compared directly to $\Delta^{14}C$ profiles of the modern ocean, since in the past, atmospheric $\Delta^{14}C$ was higher than today, and there was higher $\Delta^{14}C$ everywhere in the atmosphere and ocean. This limitation also applies for comparisons of $\Delta^{14}C_0$ across different time periods. Therefore, though $\Delta^{14}C_0$ can be used in combination with conservative tracers of circulation to assess water mass mixing lines from a single time period, the value of $\Delta^{14}C_0$ cannot be compared across different time periods.

To find a reference curve for $\Delta^{14}C_0$, we correct the modern profile ($\Delta^{14}C_B$ in equation (1)) to a world with higher atmospheric $\Delta^{14}C$, which is the radiocarbon profile ($\Delta^{14}C_A$ in equation (1)) that would have existed if the circulation in the past were identical to the modern circulation, but the ocean/atmosphere had higher $\Delta^{14}C$ everywhere than today. We include the uncertainty in the $\Delta^{14}C_{Atm}$ and the calendar age of the sample in the uncertainty of the profile. Translating the modern profile by a constant $\Delta^{14}C$ would not give the same result because of the exponential decay of ^{14}C. In the past, there would have been larger gradients in $\Delta^{14}C$, even if the gradients in radiocarbon age were identical.

2.3.3. The Anomaly of $\Delta^{14}C_0$ From the Contemporary Atmosphere ($\Delta^{14}C_{0-Atm}$)

The $\Delta^{14}C_0$ is frequently graphed with a time series of atmospheric $\Delta^{14}C$. We calculate this difference, $\Delta^{14}C_{0-Atm}$ (sometimes called $\Delta\Delta^{14}C$ in the literature), for our data using the full probability distribution of the calendar age of the sample and the uncertainty in the Intcal13 curve (Figure 3d). The reference curve for $\Delta^{14}C_{0-Atm}$ is the reference curve for $\Delta^{14}C_0$ minus the $\Delta^{14}C_{Atm}$ value at the time.

2.3.4. The Benthic-Atmosphere Age Difference (t_{B-Atm})

The $\Delta^{14}C_{0-Atm}$ can be converted into radiocarbon age, resulting in t_{B-Atm}, the benthic-atmosphere radiocarbon age difference. It is also equivalent to the difference between the measured radiocarbon age of the benthic sample minus the radiocarbon age of the contemporary atmosphere (the radiocarbon age of the planktonics minus the surface reservoir age). The advantages of t_{B-Atm} are that it is simple to calculate and its magnitude is not sensitive to the total radiocarbon budget in the atmosphere and ocean. With identical circulation, it would have the same value in the past, even with higher radiocarbon inventories. The reference curve for t_{B-Atm} is the modern radiocarbon age profile, and it is comparable across all time periods. Using t_{B-Atm} avoids the cumbersome calculation of preindustrial reference curves necessary with $\Delta^{14}C_0$ and $\Delta^{14}C_{0-Atm}$. However, it can be confusing in that its units are years, though it is neither a ventilation age nor transit time.

2.3.5. $\Delta^{14}C_0$ Corrected to the Preindustrial World ($\Delta^{14}C_{0,adj}$)

If we convert the t_{B-Atm} into units of $\Delta^{14}C$, we find the $\Delta^{14}C_{0,adj}$, which is the $\Delta^{14}C_{0-Atm}$ corrected to the value it would have in a world where atmospheric $\Delta^{14}C$ was 0‰. The reference curve is the modern $\Delta^{14}C$ profile. Like t_{B-Atm}, it has the advantage that it is comparable across all time periods. However, like all the of the radiocarbon metrics discussed so far, comparing directly to a modern, quasi-steady state profile intrinsically assumes that the past radiocarbon profile is also steady state. With varying atmospheric $\Delta^{14}C_{Atm}$ and varying circulation in the LGM and deglaciation on timescales shorter than the timescale of ocean overturning, the ocean radiocarbon field at a given time probably did not represent a steady state situation.

2.3.6. The Projection Age (t_{Proj}, t_{Proj2})

The "projection age" takes into account the changing atmospheric $\Delta^{14}C$ between the time when a water mass forms and when it reaches the deep ocean [*Adkins and Boyle*, 1997]. Because of the long-term decrease in atmospheric $\Delta^{14}C$ since the LGM, benthic foraminifera grow in water that was last in contact with the
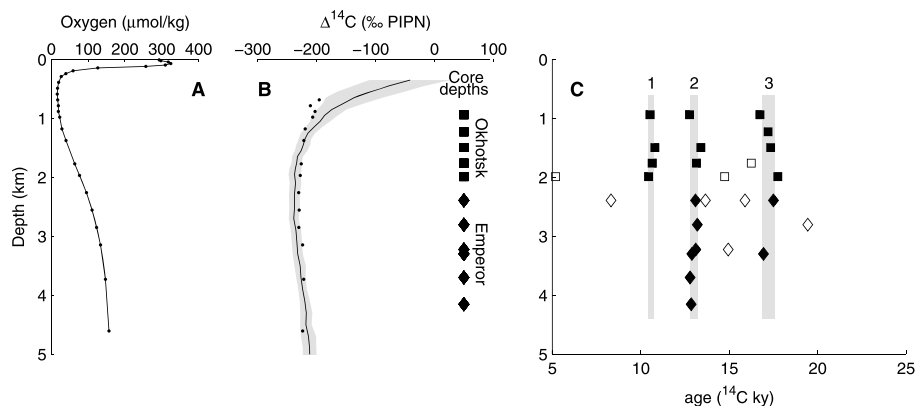
Figure 4. Hydrographic data and core depths. (a) Oxygen measured from WOCE Line P13 Station 23 (1992). (b) North Pacific mean Δ^{14}C and 1σ standard deviation (thin black line and grey shading) [*Key et al.*, 2002], plotted with the Δ^{14}C profile measured at WOCE Line P13 Station 23 (dots) and the depths of the Okhotsk and Emperor cores from this study (squares and diamonds, respectively). (c) The planktonic radiocarbon ages of peaks in *Uvigerina* abundance. Closed symbols are peaks within clusters, and open symbols are peaks outside of those clusters. The light grey shading is the weighted mean and standard deviation of the ages of abundance peaks in clusters.

atmosphere when Δ^{14}C was likely higher. Therefore, the benthic Δ^{14}C is higher than it would have been if atmospheric Δ^{14}C were constant. With this method, a benthic sample is assumed to have grown a water parcel that was a closed system after it left its formation area, so that the change in the Δ^{14}C of the parcel was solely a function of radioactive decay during transit. This is a poor assumption in most cases [*Gebbie and Huybers*, 2012].

In the original projection method, the water parcel the benthic foraminifera grew in ($\Delta^{14}C_0$) is $\Delta^{14}C_B$ in equation (1), and y is the time it takes for the decay trajectory to intersect the atmospheric Δ^{14}C curve ($\Delta^{14}C_A$). The projection age is defined as the difference between this value and the calendar age of the sample, minus the local surface reservoir age ($R + \Delta R$). The reference curve is the radiocarbon profile of the modern ocean, converted to calendar years with the true decay constant λ_C. We use a modified version of the projection age in this study. Rather than finding the intersection of the decay trajectory at the atmospheric Δ^{14}C curve, we find the intersection with the mean surface ocean [*Skinner and Shackleton*, 2004; *Lund*, 2013]. This projection method illuminates the magnitude of bias that could be introduced into a benthic foraminiferal radiocarbon measurement from atmospheric Δ^{14}C changes alone.

The transit-time distribution, equilibration-time distribution method ($t_{TTD-ETD}$) [*DeVries and Primeau*, 2010] is identical to the projection method except that it takes into account transit-time distributions to produce a mean age, which is typically lower than the projection age [*Lund*, 2013]. This is smaller than typical radiocarbon measurement uncertainty.

2.4. North Pacific Radiocarbon Compilation

We compiled North Pacific benthic-planktonic radiocarbon pairs from the literature (Table S1 in the supporting information) and calculated $\Delta^{14}C_0$ and $\Delta^{14}C_{0,adj}$ using the value of local surface reservoir age assumed in the original publications (Figures 7 and 8). The reference curve for this compilation is the *Key et al.* [2002] average North Pacific radiocarbon profile. The compilation does not include *Marchitto et al.* [2007] since it does not have any planktonic radiocarbon data, but we include planktonic-benthic pairs from *Sarnthein* [2007] and *Ikehara et al.* [2011] calculated with a constant preindustrial surface reservoir age. A comparison of the compilation to the data from these two papers with independent age models appears in the supporting information.

3. Results

3.1. Benthic Foraminiferal Abundance Peaks

In all cores, there are peaks in the absolute abundance of *Uvigerina* that rise an order of magnitude above the background (Figure 2). The ages of the abundance peaks cluster at three time periods (Figure 4c). In the
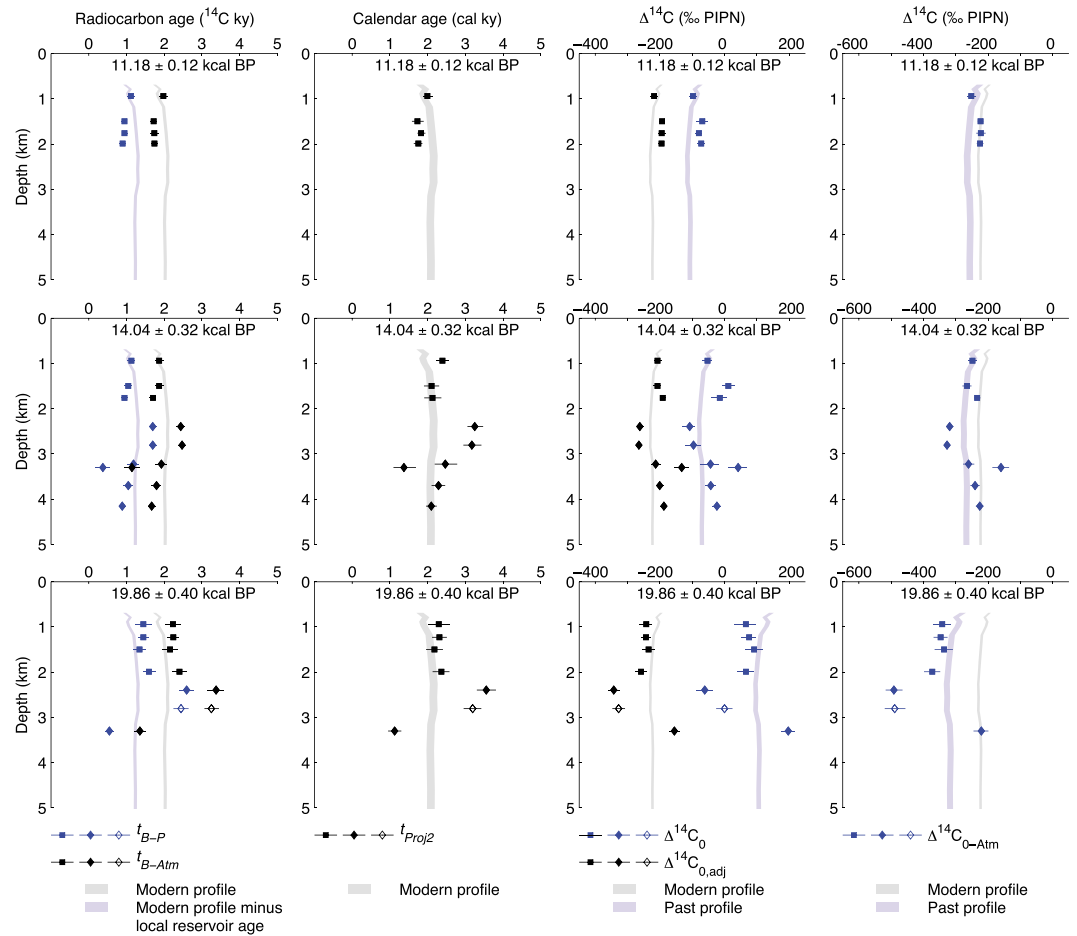
Figure 5. Radiocarbon profiles for the three time slices shown in Figure 4, using $\Delta R = 390 \pm 0$ years (surface reservoir age of 790 ± 0 years). Each row is a single time slice annotated with the calibrated calendar age of the slice, and the columns show various metrics representing radiocarbon in the past water column (from left to right) benthic-planktonic age difference t_{B-P} (blue) and benthic-atmosphere age difference t_{B-Atm} (black); the modified (see text) projection age t_{Proj} (black); the estimated benthic $\Delta^{14}C$ at the time they grew $\Delta^{14}C_0$ (blue), and that quantity corrected to a world with atmospheric $\Delta^{14}C$ of 0‰ $\Delta^{14}C_{0,adj}$ (black); the difference between the benthic $\Delta^{14}C$ and the contemporary atmosphere $\Delta^{14}C_{0-Atm}$. The open symbols show the data point from 76 cm in RNDB GGC5 which falls in the LGM but is not in the LGM abundance peak cluster. The Okhotsk and Emperor data are in squares and diamonds, respectively. The WOCE P13 Station 23 profile is shown in grey, and that profile corrected to a world with higher past atmospheric $\Delta^{14}C$ is in blue. The same figure but using other values of ΔR are in the supporting information. The error bars are 1σ, and the width of the water column profiles are 1σ.

Okhotsk Sea, there is a peak that appears at $10{,}610 \pm 150$ [14]C years from four cores spanning 939 to 1990 m water depths. In all cores from the Okhotsk Sea and Emperor Seamounts, there is another peak that appears at $13{,}030 \pm 210$ [14]C years. During the LGM there is a looser cluster at $17{,}250 \pm 360$ [14]C years. The LGM, defined as the maximum benthic $\delta^{18}O$, falls between 70 and 240 cm in the cores (Figure 2). Sediment accumulation rate ranges from around 5 to 15 cm/kyr. Cores RNDB-GGC15 and VINO-GGC17 had incomplete stable isotope stratigraphies due to the low abundance of benthic foraminifera.

The abundance peaks in our cores probably represent discrete time periods of higher productivity which were subsequently bioturbated. This is most clearly seen in cores RNDB PC11 and VINO19-4 GGC37 (Figure 2), since each has a single abundance peak. The shape and width of the abundance peaks are consistent with mixing of an originally narrow peak, with a longer tail upcore in abundance [*Berger and Heath*, 1968]. There are local abundance maxima within the broader abundance peak where benthic and planktonic ^{14}C measurements are within error (Table 2 and Figure 2), and the benthic $\delta^{18}O$ also plateau during the abundance peaks.
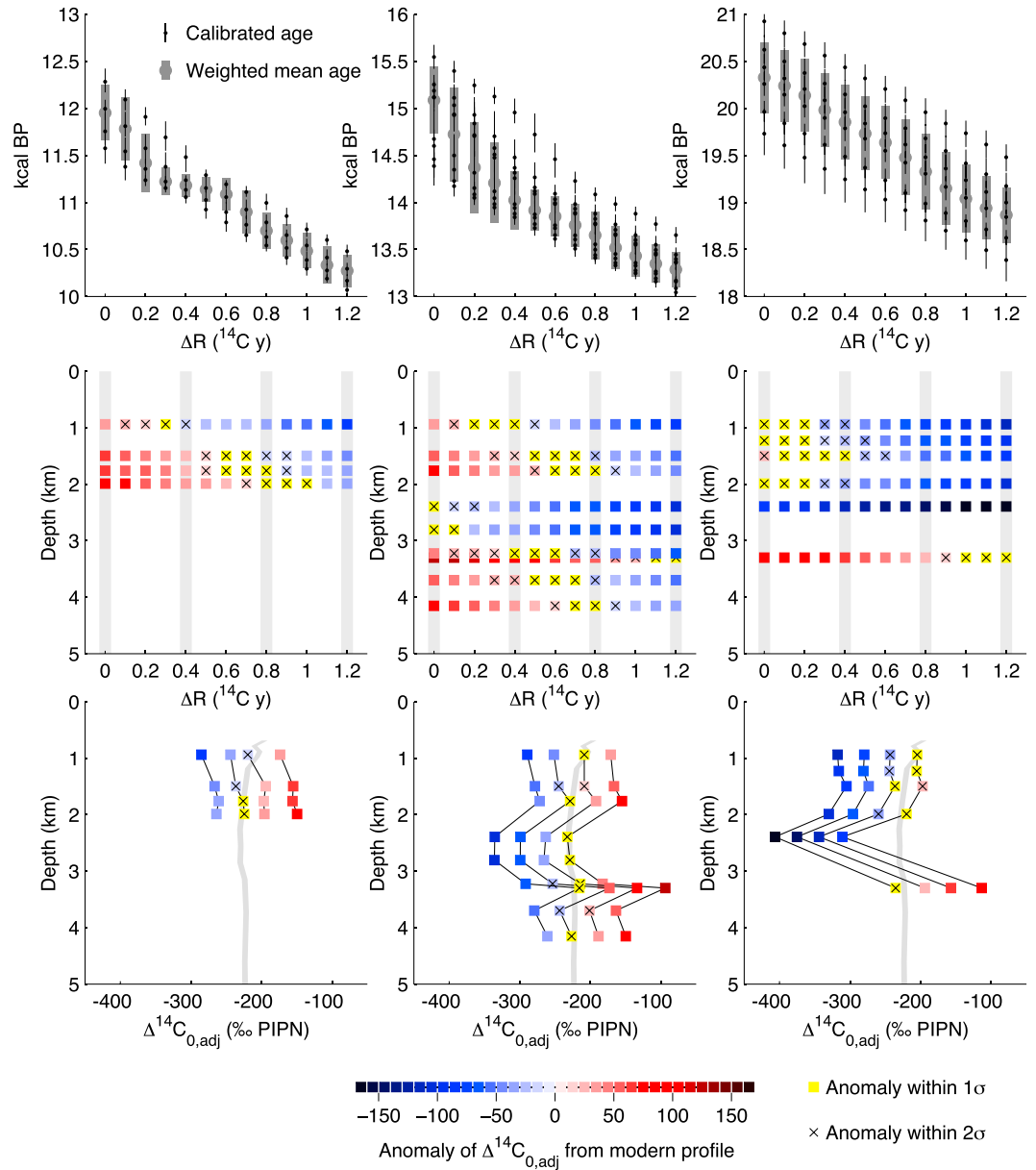
Figure 6. The effect of assumed surface reservoir age on the time slice ages and radiocarbon estimates. (top row) The calibrated calendar ages for the points in each time slice, and the weighted mean calendar age. Error bars are 1σ. (middle row) The difference between $\Delta^{14}C_{0,adj}$ and the modern profile. For each time slice, the vertical structure is independent of ΔR, but the absolute value of $\Delta^{14}C_{0,adj}$ depends on ΔR. The grey bars indicate the four profiles illustrated in the bottom row. (bottom row) The modern profile at WOCE P13 Station 23 (grey) and the four profiles calculated with ΔR of 0, 400, 800, and 1200 years.

3.2. Radiocarbon Analysis

All five metrics show approximately the same relative vertical structure of radiocarbon in the water column, and with the exception of the projection age, they show the same relative enrichment/depletion in radiocarbon relative to the reference curve for the modern ocean (Figure 5). This includes the $\Delta^{14}C_{0-Atm}$ profiles, which show larger gradients than the $\Delta^{14}C_{0,adj}$ profiles (Figure 5 and Table S1) but are consistent with the preindustrial reference curve that accounts for higher past ^{14}C. The t_{Proj2} is consistently higher than the t_{B-Atm} because of the generally decreasing $\Delta^{14}C_{atm}$ through time. With constant $\Delta^{14}C_{atm}$, the t_{Proj2} and t_{B-Atm} would be proportional by a factor of the ratio of λ_L and λ_C.
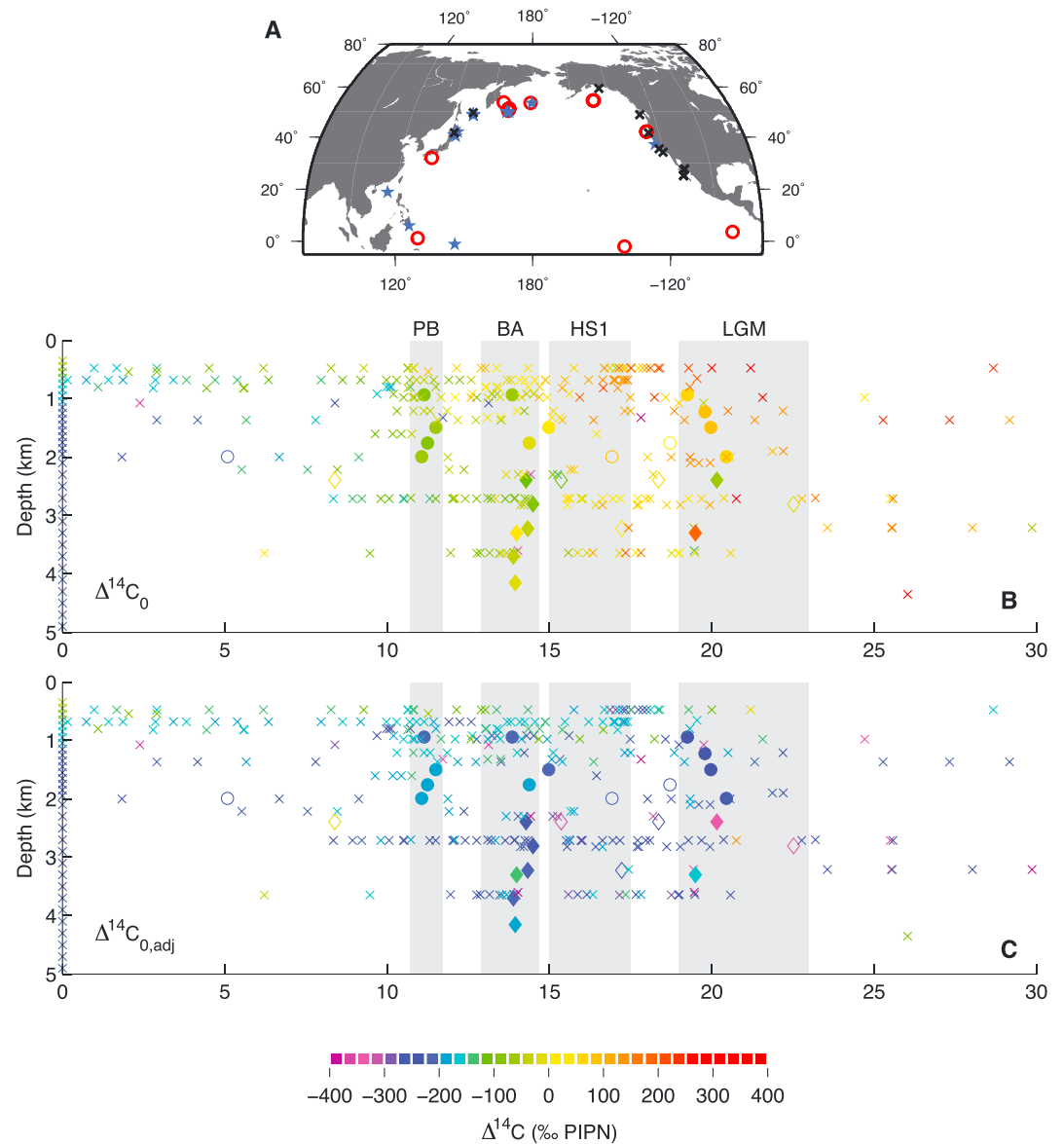
Figure 7. Compilation of planktonic-benthic radiocarbon data from the North Pacific (data tabulated in the supporting information). (a) Map of core locations color coded by water depth, >2500 m is red, 1000 to 2500 m is blue, <1000 m is black. (b) The $\Delta^{14}C_0$ and (c) $\Delta^{14}C_{0,adj}$, plotted by calendar age and water depth. We used constant surface reservoir ages from the original publications. The grey bars show the Preboreal, Bolling-Allerod (BA), Heinrich Stadial 1 (HS1), and Last Glacial Maximum (LGM) time slices shown in Figure 8. The compilation data are marked with crosses. The data from this study are in circles (Okhotsk) and diamonds (Emperor), where points from abundance peak clusters are solid, points outside clusters are open.

Using the constant preindustrial surface reservoir age (790 years, or $\Delta R = 390$ years) (Figure 5), the early Preboreal $\Delta^{14}C$ profile is similar to today at 940 m water depth but significantly enriched in radiocarbon at 1–2 km water depth. During the early Bolling, the $\Delta^{14}C$ profile is similar to today at 939 m and 2–3 km water depth, but it is significantly enriched at 1–2 km and greater than 3 km water depth. During the LGM, the $\Delta^{14}C$ values in the profile are similar or slightly lower than today, except greater than 2.5 km water depth, where one estimate from 19.9 ± 0.2 kcal B.P. at 2400 m water depth is depleted in ^{14}C compared to the modern profile, and another estimate from 19.3 ± 0.3 kcal B.P. at 3300 m water depth is enriched (Figure 5).

The ages of the time slices (Figure 6, top row) and the relative enrichment/depletion of the water column in radiocarbon compared to the modern ocean (Figure 6, bottom row) depend on the surface reservoir age
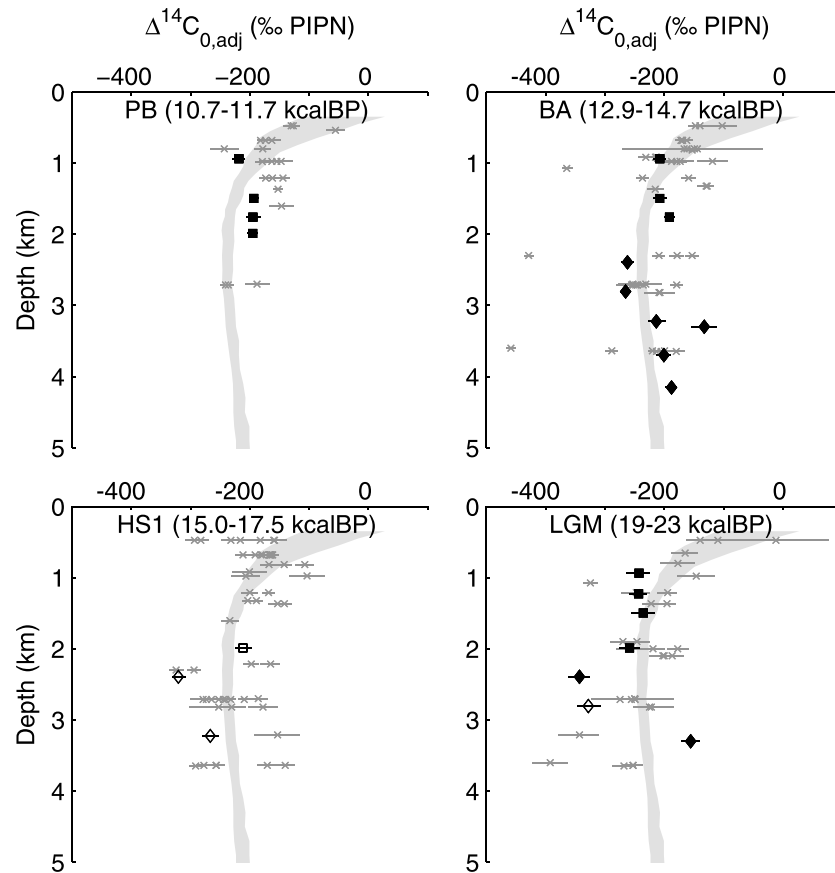
Figure 8. Compilation of radiocarbon data from the subarctic Pacific. Time slices are from the grey bars in Figure 7c. The grey curve is the mean North Pacific radiocarbon from *Key et al.* [2004]. Grey crosses are published data from the literature. NW Pacific data from this study are in black squares (Okhotsk) and diamonds (Emperor), where points from abundance peak clusters are solid, points outside clusters are open. The error bars are 1σ. See Table S1 in the supporting information for the citations for the complied data.

assumed. The calendar age of a sample can be very sensitive to the surface reservoir age if it intersects the calibration curve at a time when $\Delta^{14}C$ is changing rapidly, and because of the exponential decay of ^{14}C, the calculated $\Delta^{14}C_0$ is very sensitive to age. With larger surface reservoir age the resulting calendar age of the sample is lower, resulting in lower $\Delta^{14}C_0$ for a sample. This in turn results in a greater difference between $\Delta^{14}C_0$ and the contemporary atmosphere, $\Delta^{14}C_{0-Atm}$, and a lower $\Delta^{14}C_{0, adj}$. Figure 6 illustrates this effect. Whatever metric is used, the radiocarbon estimate of the water column is lower (more depleted in radiocarbon) with larger surface reservoir age, and higher (more enriched in radiocarbon) with a smaller surface reservoir age.

Increasing the surface reservoir age does not affect t_{B-P}, since the quantity does not take it into account, but it moves the modern reference curve to lower values, making the t_{B-P} values higher relative to the reference curve. For t_{Proj2}, higher surface reservoir age decreases the calendar age of the sample, increasing the difference between the age of the sample and the intersection of the decay curve with the surface ocean. As mentioned above, t_{Proj2} systematically results in a larger ventilation age than t_{B-P} for most time periods because of the generally decreasing $\Delta^{14}C_{atm}$ through time. This effect is amplified when the sample age is on the order of 1000 years after a time when $\Delta^{14}C_{atm}$ is decreasing rapidly, notably, during H1 and Younger Dryas.

In Figure 7, we compile published radiocarbon data from across the North Pacific, using the constant surface reservoir age used in the original publications. Figure 7b shows the generally decreasing $\Delta^{14}C_0$ in the ocean with decreasing atmospheric $\Delta^{14}C$. The $\Delta^{14}C_{0,adj}$ (Figure 7c) can be interpreted as a rough correction for this effect.

Figure 8 shows profiles from four time periods, the early Holocene (10.7–11.7 kcal B.P.), the Bolling-Allerod (BA) (12.9–14.7 kcal B.P.), the Heinrich Stadial 1 (HS1) (15.0–17.5 kcal B.P.), and the LGM (19–23 kcal B.P.). Compiling data from an ocean basin from a time period longer than 1000 years onto a single profile inevitably introduces noise due to real spatial and temporal heterogeneity but can be useful for seeing the shape of the profile. Each profile contains scatter of up to 200‰, and the BA profile also contains three points that have $\Delta^{14}C_{0,adj}$ less than −300‰, which are from the Japan Margin [*Ikehara et al.*, 2011], the Emperor Seamounts [*Sarnthein et al.*, 2007], and the south-central Bering Sea [*Gorbarenko*, 2005]. These points are arguably outliers.

The LGM profile (Figure 8c) is similar to the modern profile above 2 km. Below 2 km, the estimates are quite variable, with the highest values similar to the water at 1–2 km, and the lowest values 100–200‰ lower. This is consistent with the presence of a poorly ventilated, low-$\Delta^{14}C$ water mass present at least in some areas of the deep North Pacific in this time interval.

The shapes of the profiles from HS1 and the BA are clearly different than the LGM, where there is a minimum in $\Delta^{14}C_{0,adj}$ at 2–3 km water depth, and slightly higher values below, similar in shape to the modern profile. During the early Holocene (Figure 8a), there are fewer data, which also appear similar to the modern profile.

4. Discussion

4.1. Productivity Peaks

Deglacial productivity maxima in the North Pacific [*Keigwin*, 1998; *Crusius et al.*, 2004; *Kohfeld and Chase*, 2011] have the fortuitous effect of creating high abundance of foraminifera in the Okhotsk and Emperor sediment cores. This enabled us to create time slices of radiocarbon from the high-productivity time from this small geographic area. Benthic foramininiferal production rate is observed to respond to increased export production at seasonal and interannual timescales [*Altenbach*, 1992; *Gooday*, 2002] and probably represents a response of the benthic ecosystem to high export production. Bias in measured radiocarbon due to bioturbation and changing abundance is minimized by analyzing samples from the top of abundance peaks [*Broecker et al.*, 1984], resulting in robust ages even though the sediment accumulation rates are not very high.

The *Uvigerina* abundance peak during the early Bolling is seen in all of the Okhotsk and Emperor sediment cores, from 939 to 4155 m water depth in both the coring areas (Figure 2) (it was too small to date in NES25-1 GGC15 but dated in all the other cores). These abundance peaks that cluster in time from sediment cores of varying depth in the same geographic region mostly likely represent the same high-productivity event; and therefore, the time slices reveal a snapshot of the radiocarbon distribution in the water column during the event.

The timing of the deglacial peaks in benthic foraminiferal abundance is consistent with the compilation of subarctic Pacific productivity proxy records by *Kohfeld and Chase* [2011], which show elevated flux of organic carbon and biogenic carbonate across the NW Pacific at these times. During the Preboreal, the abundance peak is only observed in Okhotsk Sea sediment cores, suggesting that high export production was limited to the Okhotsk Sea, or that it occurred in both areas, but with a lower magnitude than the Bolling, and the organic matter flux was completely consumed by water column respiration above 2 km, the shallowest of the Emperor sediment cores, or that the sediment accumulation rates before 12 ka at the Emperor sites was lower.

The duration of these high-productivity events is not well constrained since the cores have relatively low sediment accumulation rates, and the width of the sediment interval that is enriched in biogenic components could be increased by bioturbation after deposition. The identical (within measurement error) planktonic radiocarbon ages measured centimeters apart at the top of the peaks RNDB PC11 and VINO19-4 GGC37 (as discussed above) suggest that the peak in foraminiferal accumulation rate may have been brief and accurately radiocarbon dated. In this case, the variation in planktonic ages for each cluster of abundance peaks would result from asynchrony of the productivity events.

We did not measure planktonic abundance, but it appears to peak with the benthics [*Keigwin*, 1998]. If planktonic and benthic foraminiferal abundance maxima are not synchronous, the planktonic date would be

biased by bioturbation. Alternatively, the measured age for each abundance peak is the weighted mean age from a longer interval of elevated foraminiferal accumulation that was subsequently homogenized by bioturbation. The planktonic age could also be biased by differential preservation during bioturbation [*Barker et al.*, 2007]. Regardless, the Preboreal and Bolling time slices represent the high-productivity time period and the water column radiocarbon distribution in that regime. For the LGM cluster, the wider range in planktonic radiocarbon ages indicates that this "time slice" may actually represent a longer time period where there may have been time variation in the water column hydrography.

Since the deglacial productivity maxima are observed across the subarctic Pacific [*Kohfeld and Chase*, 2011], there is potential for more benthic-planktonic radiocarbon measurements from during the same events in other sediment cores. This includes sediment cores, like from the present study in the NW Pacific, which have relatively low sediment accumulation rates and would otherwise be unsuitable for making time slices from millennial-scale climate events. Comparison of data from these events could provide a three-dimensional view of the radiocarbon activity of the subarctic Pacific water column during these high-productivity episodes.

4.2. The Local Surface Reservoir Age Problem

Changes in atmospheric production rate and ocean circulation affect surface reservoir ages globally. In an experiment testing the effect of changing $\Delta^{14}C_{atm}$ on surface reservoir ages, surface reservoir age varied globally at centennial to millennial timescales, by up to 300 years [*Franke et al.*, 2008]. As the atmospheric $\Delta^{14}C$ varied, the lag in surface ocean $\Delta^{14}C$ changes caused higher surface reservoir ages with increasing $\Delta^{14}C_{atm}$ and lower surface reservoir ages with decreasing $\Delta^{14}C_{atm}$. In another experiment a 30% weaker export of deep water (and ^{14}C) resulted in globally increased surface ocean age, by up to 200–300 years [*Franke et al.*, 2008]. The magnitude and pattern of surface reservoir age changes in these experiments are similar to other studies [*Butzin et al.*, 2005; *Ritz et al.*, 2008]. During the deglaciation, atmospheric $\Delta^{14}C$ and air-sea carbon dioxide exchange were closely linked [*Hughen et al.*, 2000; *Broecker and Barker*, 2007], and the reservoir age effects of each mechanism would be superposed.

We assumed that the local surface reservoir ages were uniform across our study area. If the surface reservoir age in the Okhotsk Sea changed independently from that at the Emperor Seamounts, this would result in biases that would affect the age and radiocarbon activity estimates from those two coring areas differently. This is a possibility we cannot test at this time, since we do not have independent age control for these sediment cores. However, the calibrated planktonic radiocarbon ages of the Okhotsk and Emperor abundance peaks do not show systematic differences between the two sites.

In the NW Pacific, using the preindustrial estimate of local ΔR of 390 years (surface reservoir age of 790 years), the Preboreal water column at 1–2 km is significantly ($>2\sigma$) enriched in radiocarbon compared to the modern (Figures 5 and 6), but with a ΔR of 700 years (surface reservoir age of 1100 y), it is indistinguishable from the modern profile (within 1σ) (Figure 6). For the Bolling-Allerod, the water column at 1–2 km and 2–3 km is similar and depleted in radiocarbon compared to the modern, respectively, but deeper than 3 km, it is enriched in radiocarbon with a ΔR of 390 years (surface reservoir age of 790 years), and indistinguishable from the modern with a ΔR of 700 years (surface reservoir age of 1100 years). These interpretations do not depend on the radiocarbon activity metric used, the $\Delta^{14}C_0$, $\Delta^{14}C_{0-Atm}$, and $\Delta^{14}C_{0,adj}$ profiles all show the same pattern relative to their respective reference curves (Figure 5). Since a change in surface reservoir age of a few hundred years is in the range that may reasonably be expected to have occurred during the deglaciation, it is difficult to say with confidence what the absolute value of the water column $\Delta^{14}C$ was in the past.

However, we find that the shape of the reconstructed radiocarbon activity profile is not sensitive to the surface reservoir age used (Figure 6; see animation S1 in the supporting information). There are only small differences in the radiocarbon profiles between those calculated with different surface reservoir age, attributable to changes in slope in the Intcal13 data set. This result is important because it shows that even with unknown surface reservoir age, if we can assume that the abundance peaks that we radiocarbon dated are coeval, we can reconstruct the shape of the radiocarbon profile, even if we do not know its absolute value. Given that the observed productivity maxima from the last deglaciation are widespread across the subarctic Pacific, it presents the valuable opportunity for similar reconstructions from depth transections of sediment cores from other locations.

COOK AND KEIGWIN   189

Table 4. Radiocarbon Calculations Using $\Delta R = 390$ Years (Surface Reservoir Age of 790 Years) With 1-Sigma Uncertainties (Figure 4)

Core Name	Water Depth (m)	Core Depth (cm)	Peak #	Calendar Age (kcal B.P.)	t_{B-P} (^{14}C ky)	t_{B-Atm} (cal ky)	$\Delta^{14}C_0$ (‰)	$\Delta^{14}C_{0-Atm}$ (‰)	$\Delta^{14}C_{0,adj}$ (‰)	t_{Proj2} (cal ky)
NES25-1 GGC27	995	41.5–42.5	1	11.14 ± 0.07	1.12 ± 0.10	1.98 ± 0.12	−98 ± 12	−252 ± 14	−218 ± 12	1.99 ± 0.13
		47.0–49.0	2	13.85 ± 0.08	1.13 ± 0.11	1.87 ± 0.12	−53 ± 14	−248 ± 14	−208 ± 11	2.39 ± 0.17
B34-91		69.0–71.0	3	19.26 ± 0.25	1.45 ± 0.22	2.24 ± 0.22	66 ± 35	−342 ± 27	−242 ± 21	2.30 ± 0.30
	1227	224.0–226.0	3	19.80 ± 0.13	1.45 ± 0.14	2.24 ± 0.16	76 ± 22	−347 ± 22	−243 ± 15	2.31 ± 0.20
NES25-1 GGC20	1510	143.0–144.0	1	11.50 ± 0.16	0.95 ± 0.07	1.73 ± 0.08	−69 ± 19	−223 ± 9	−193 ± 8	1.73 ± 0.16
		179.0–181.0	2	14.97 ± 0.14	1.05 ± 0.10	1.87 ± 0.12	12 ± 20	−265 ± 15	−208 ± 12	2.11 ± 0.20
		229–231	3	19.97 ± 0.15	1.35 ± 0.17	2.16 ± 0.21	91 ± 27	−336 ± 29	−235 ± 20	2.18 ± 0.22
NES25-1 GGC18	1700	143.0–145.0	1	11.25 ± 0.07	0.95 ± 0.07	1.74 ± 0.12	−80 ± 10	−223 ± 15	−195 ± 12	1.83 ± 0.11
		167.0–169.0	2	14.39 ± 0.22	0.95 ± 0.08	1.71 ± 0.09	−15 ± 26	−234 ± 10	−191 ± 9	2.13 ± 0.24
		215.0–217.0		18.72 ± 0.12	1.55 ± 0.18	2.35 ± 0.20	49 ± 24	−357 ± 27	−254 ± 19	2.29 ± 0.25
NES25-1 GGC15	1980	29.0–31.0		5.09 ± 0.11	1.65 ± 0.06	2.36 ± 0.07	−210 ± 9	−271 ± 7	−255 ± 6	2.27 ± 0.10
		72.0–73.0	1	11.07 ± 0.08	0.90 ± 0.09	1.74 ± 0.09	−72 ± 12	−225 ± 10	−195 ± 9	1.76 ± 0.12
		131.0–132.0		16.93 ± 0.14	1.10 ± 0.11	1.91 ± 0.14	77 ± 22	−289 ± 19	−211 ± 14	1.78 ± 0.16
		169.0–171.0	3	20.45 ± 0.14	1.60 ± 0.16	2.41 ± 0.19	66 ± 25	−373 ± 26	−259 ± 18	2.37 ± 0.22
RNDB PC13	2329	15.0–17.0		8.39 ± 0.04	−0.63 ± 0.06	0.12 ± 0.09	59 ± 8	−15 ± 12	−14 ± 11	−0.24 ± 0.08
		53.0–55.0	2	14.28 ± 0.18	1.70 ± 0.10	2.44 ± 0.12	−108 ± 22	−319 ± 12	−262 ± 11	3.25 ± 0.22
		60.5–61.5		15.36 ± 0.16	2.34 ± 0.12	3.10 ± 0.14	−124 ± 20	−414 ± 15	−320 ± 12	3.47 ± 0.18
		79.0–82.0		18.36 ± 0.10	1.45 ± 0.11	2.25 ± 0.14	63 ± 18	−343 ± 18	−244 ± 13	2.07 ± 0.16
		100.0–101.0	3	20.16 ± 0.15	2.60 ± 0.19	3.38 ± 0.22	−61 ± 25	−491 ± 27	−343 ± 18	3.56 ± 0.26
RNDB GGC5	2804	31.0–32.0	2	14.50 ± 0.24	1.70 ± 0.09	2.48 ± 0.09	−96 ± 27	−327 ± 9	−265 ± 9	3.18 ± 0.25
		75.0–77.0		22.52 ± 0.13	2.45 ± 0.20	3.20 ± 0.24	0 ± 26	−489 ± 33	−328 ± 20	3.26 ± 0.20
RNDB PC11	3225	71.5–72.5, 75.5–76.5	2	14.34 ± 0.24	1.19 ± 0.15	1.93 ± 0.16	−44 ± 31	−261 ± 18	−213 ± 16	2.47 ± 0.31
VINO19-4 GGC37	3300	108.0–109.0		17.23 ± 0.15	1.70 ± 0.14	2.49 ± 0.16	12 ± 22	−368 ± 20	−266 ± 14	2.39 ± 0.22
		49.0–51.0, 55.0–57.0	2	13.99 ± 0.15	0.38 ± 0.20	1.15 ± 0.21	42 ± 29	−160 ± 27	−133 ± 23	1.37 ± 0.32
RNDB GGC15	3700	117.0–118.0	3	19.50 ± 0.11	0.55 ± 0.12	1.36 ± 0.16	197 ± 21	−221 ± 24	−155 ± 17	1.13 ± 0.18
		29.0–30.0	2	13.89 ± 0.08	1.05 ± 0.12	1.80 ± 0.12	−43 ± 16	−240 ± 15	−201 ± 12	2.29 ± 0.18
VINO19-4 GGC17	3950	90.0–95.0	2	13.95 ± 0.07	0.89 ± 0.09	1.67 ± 0.10	−24 ± 13	−226 ± 12	−188 ± 10	2.10 ± 0.15

4.3. Radiocarbon Metrics

With the exception of the projection age (t_{Proj2}), all of the radiocarbon metrics (t_{B-P}, t_{B-Atm}, $\Delta^{14}C_0$, $\Delta^{14}C_{0-Atm}$, and $\Delta^{14}C_{0,adj}$) show the same relationship to the modern reference curve for our NW Pacific data set (Figure 5). This demonstrates that though the metrics vary in frame of reference (surface ocean and atmosphere) and unit (^{14}C years, permil), the result (relative enrichment or depletion in radiocarbon in the past compared to today) is the same as long as they are compared to the appropriate reference curve.

The t_{Proj2} (with or without the transit-time distribution correction of *DeVries and Primeau* [2010]) is frequently greater than t_{B-Atm} because of the generally decreasing $\Delta^{14}C_{Atm}$ through the deglaciation (Table 4 and Figure 5). Therefore, the interpretation of t_{B-Atm} and t_{Proj2} should be made carefully keeping in mind that the former does not include the effects of past higher $\Delta^{14}C_{Atm}$, and that the latter includes the assumption that the benthic foraminifera grew in water with a single source. Because of this inherent assumption, the projection age method can only be strictly applied in areas where one water mass dominates the composition, and the main influence on subsurface radiocarbon is transit time of that water mass, not changes in the end-member water masses or their mixing ratio.

Though the dominant source of water in the deep Pacific through the last glacial cycle appears to be the Southern Ocean [*Adkins*, 2013], it is probably a poor assumption that the ratio of constituent water masses did not change through time. The glacial ocean appeared much more stratified than today, with a strong divide between the deep ocean (southern source) and upper ocean (northern source) [*Adkins*, 2013]. In contrast, ~30% of the water in the deep North Pacific today (>2 km) originates from the Arctic and North Atlantic [*Gebbie and Huybers*, 2010] and is entrained into deep Pacific water through mixing in the Southern Ocean. In addition, if modern North Pacific Intermediate Water was replaced with a glacial North Pacific Deep Water during the LGM and deglaciation [*Horikawa et al.*, 2010; *Okazaki et al.*, 2010, 2014; *Rae et al.*, 2014], then the projection age method probably cannot be applied at all, since the end-members are changing through time.

4.4. Pacific Ventilation Changes

The Okhotsk Sea LGM radiocarbon estimates indicate water similar or radiocarbon depleted compared to the modern water column (Figure 5). The considerable difference in the two radiocarbon estimates >2 km from the LGM cluster at the Emperor Seamounts (VINO19-4 GGC37 and RNDB PC13) is puzzling since these two cores are close to each other. The calendar ages of the two data points are 600 years apart, so they could be the result of real variations in radiocarbon through time. Looking at these data points in the context of the North Pacific compilation (Figure 8), we see scatter of a similar magnitude for points from this 4000 year length of the interval designated as the LGM, which could also be from temporal variations. Another possibility is that it could also reflect spatial variation in the boundary between radiocarbon-enriched and radiocarbon-depleted water and horizontal gradients in radiocarbon activity across the North Pacific basin. There are too few data to assess spatial or temporal relationships between the lower and higher points.

By the BA, this pattern has clearly changed, where all but three of the estimates indicate water similar to or slightly enriched in radiocarbon compared to the modern water column >2 km (Figure 5). The shape of the BA profile in the NW Pacific and the North Pacific compilation is similar to the modern profile, with fairly uniform values deeper than 1 km water depth, and possibly a minimum in radiocarbon (maximum in age) in middepths, at around 2–3 km (Figure 8). This is consistent with a modern-like circulation established in North Pacific by this time period.

The LGM radiocarbon profile is consistent with *Cibicidoides* $\delta^{13}C$ [*Herguera et al.*, 1992; *Keigwin*, 1998; *Matsumoto et al.*, 2002] data that suggest relatively poorly ventilated water >2 km and better-ventilated water above 2 km during the LGM. The change from radiocarbon-depleted to radiocarbon-enriched water >2 km from the LGM to the Bolling-Allerod is consistent with the interpretation of *Galbraith et al.* [2007] that the poorly ventilated deep water became better ventilated during the deglaciation.

Even though there are many unconstrained mechanisms that can affect the radiocarbon activity of the water column, we can gain some insight into surface reservoir ages and ventilation of the North Pacific by comparing the NW Pacific records to benthic-planktonic foraminiferal radiocarbon data from the rest of the North Pacific (Figure 8). We assumed constant surface reservoir age for each site in these calculations. Changing surface reservoir age at a given site will bias the radiocarbon activity estimate. Some of the scatter

in the compilation could be therefore be from varying surface reservoir age across sites for a given time slice. Despite these potential sources of variation, the $\Delta^{14}C_{0,adj}$ values in the compilation are similar in magnitude and shape to the NW Pacific data points.

The similarity of the NW Pacific profiles and the North Pacific compilation in the time slices suggests that surface reservoir age difference between the preindustrial and the past at these coring locations may have been relatively spatially coherent across the North Pacific. Since cores of similar depth were widely distributed (Figure 7a), a regional bias in surface reservoir age should not affect the shape of the profile. A systematic bias in the magnitude of global surface reservoir age between the preindustrial and the past would translate the entire radiocarbon activity compilation to higher or lower values.

There are very few radiocarbon records from the North Pacific with independent chronologies [e.g., *Marchitto et al.*, 2007; *Sarnthein et al.*, 2007; *Ikehara et al.*, 2011]. Many more of such records will be required to test the fidelity of the radiocarbon-based circulation reconstructions in this paper and other studies, and also to study the pattern and magnitude of ΔR changes through time. The numerous volcanic arcs around the North Pacific margin hold the promise of using tephrochronology to independently date sediments using tephra layers that have been dated on land [*Misarti et al.*, 2012; *Smith et al.*, 2013], a technique that has been applied to sites in the North Pacific [*Ikehara et al.*, 2011], South Pacific [*Sikes et al.*, 2000], and North Atlantic [*Bard et al.*, 1994; *Austin et al.*, 2006].

5. Conclusions

Benthic foraminifera reach peak abundance in the Okhotsk Sea and Emperor Seamounts at times during the LGM and deglaciation. Most likely this is the consequence of higher export production during the last deglaciation in the subarctic Pacific. Radiocarbon dating planktonic foraminifera from these abundance peaks shows that the peaks cluster during the LGM, the middeglaciation (Bolling-Allerod), and the early Holocene (Preboreal). The radiocarbon measurements of benthic foraminifera provided an opportunity to reconstruct ocean ventilation for those times.

We evaluated several metrics for quantifying the radiocarbon activity of the past water column. When compared to the appropriate reference curves of the modern radiocarbon profile, the t_{B-P}, t_{B-Atm}, $\Delta^{14}C_0$, $\Delta^{14}C_{0-Atm}$, and $\Delta^{14}C_{0,adj}$, all show the same relative enrichment/depletion from the appropriate reference curve for each metric. Because of generally decreasing $\Delta^{14}C_{Atm}$, t_{Proj2} is usually larger than t_{B-Atm}. Interpretation of t_{Proj2} should take into account the inherent assumption of a single water mass source area. Interpretation of all of these metrics with respect to past ventilation should be made with caution, since radiocarbon activity of the water column can be affected not only by transit time but also changing water mass source end-member compositions and mixing ratios.

Estimates of the absolute value of the water column radiocarbon activity are very sensitive to the local surface reservoir age, which is unconstrained for these samples. However, the shapes of the profiles are not sensitive to the reservoir age used, and we find that by the Bolling-Allerod the radiocarbon profile of the NW subarctic Pacific is similar to the modern profile, where there is a minimum $\Delta^{14}C$ at 2–3 km water depth and higher values above and below. A compilation of paired benthic-planktonic measurements from across the North Pacific produces vertical profiles of radiocarbon activity that are similar to the NW Pacific, suggesting that any surface reservoir age changes during the deglaciation may have been coherent across the North Pacific, though this speculation will need to be confirmed by independent estimates of surface reservoir age from the past.

The North Pacific compilation profiles suggest that waters >2 km water depth changed from being relatively radiocarbon depleted during the LGM to being relatively radiocarbon-enriched during the Bolling-Allerod. This is consistent with a relatively poorly ventilated water mass being replaced by a better-ventilated water mass over this time period. However, there is considerable scatter in the data compilation that may be due to unaccounted-for changes in surface reservoir age, spatial and temporal heterogeneity in the radiocarbon activity of the water column. In addition, the relative enrichment or depletion of the water column compared to today could be systematically biased by globally coherent changes in surface reservoir age. Ultimately, precise estimates of the $\Delta^{14}C$ of the water column and the contribution of ventilation to that $\Delta^{14}C$ will require constraints on end-member water mass $\Delta^{14}C$, mixing ratios, and local surface reservoir age.

References

Adkins, J. F. (2013), The role of deep ocean circulation in setting glacial climates, *Paleoceanography*, 28, 539–561, doi:10.1002/palo.20046.

Adkins, J. F., and E. A. Boyle (1997), Changing atmospheric Delta C-14 and the record of deep water paleo-ventilation ages, *Paleoceanography*, 12, 337–344, doi:10.1029/97PA00379.

Ahagon, N., K. Ohkushi, M. Uchida, and T. Mishima (2003), Mid-depth circulation in the northwest Pacific during the last deglaciation: Evidence from foraminiferal radiocarbon ages, *Geophys. Res. Lett.*, 30(21), 2097, doi:10.1029/2003GL018287.

Altenbach, A. V. (1992), Short term processes and patterns in the foraminiferal response to organic flux rates, *Mar. Micropaleontol.*, 19(1), 119–129.

Austin, W., J. Hunt, D. Kroon, and J. Peacock (2006), The C-14 age of the Icelandic Vedde Ash: Implications for Younger Dryas marine reservoir age corrections, *Radiocarbon*, 37(1), 53–62.

Bard, E. (1988), Correction of accelerator mass spectrometry ¹⁴C ages measured in planktonic foraminifera: Paleoceanographic implications, *Paleoceanography*, 3, 635–645, doi:10.1029/PA003i006p00635.

Bard, E., J. Mangerud, M. Paterne, L. Labeyrie, J. Duprat, and M. Mi (1994), The North Atlantic atmosphere-sea surface ¹⁴C gradient during the Younger Dryas climatic event, *Earth Planet. Sci. Lett.*, 126, 275–287.

Barker, S., W. Broecker, E. Clark, and I. Hajdas (2007), Radiocarbon age offsets of foraminifera resulting from differential dissolution and fragmentation within the sedimentary bioturbated zone, *Paleoceanography*, 22, PA2205, doi:10.1029/2006PA001354.

Berger, W. H., and G. R. Heath (1968), Vertical mixing in pelagic sediments, *J. Mar. Res.*, 16(2), 134–143.

Broecker, W., and S. Barker (2007), A 190‰ drop in atmosphere's Δ¹⁴C during the "Mystery Interval"(17.5 to 14.5 kyr), *Earth Planet. Sci. Lett.*, 256(1), 90–99.

Broecker, W., and E. Clark (2010), Search for a glacial-age ¹⁴C-depleted ocean reservoir, *Geophys. Res. Lett.*, 37, L13606, doi:10.1029/2010GL043969.

Broecker, W., A. Mix, M. Andree, and H. Oeschger (1984), Radiocarbon measurements on coexisting benthic and planktonic foraminifera shells: Potential for reconstructing ocean ventilation times over the past 20,000 years, *Nucl. Instrum. Methods Phys. Res. B*, 5, 331–339.

Broecker, W., A. Virgilio, and T.-H. Peng (1991), Radiocarbon age of waters in the deep Atlantic revisited, *Geophys. Res. Lett.*, 18(1), 1–3, doi:10.1029/90GL02707.

Broecker, W., S. Barker, E. Clark, I. Hajdas, G. Bonani, and L. Stott (2004), Ventilation of the glacial deep Pacific Ocean, *Science*, 306, 1169–1172.

Brunelle, B. G., D. Sigman, S. Jaccard, L. Keigwin, B. Plessen, G. Schettler, M. Cook, and G. Haug (2010), Glacial/interglacial changes in nutrient supply and stratification in the western subarctic North Pacific since the penultimate glacial maximum, *Quat. Sci. Rev.*, 29(19–20), 2579–2590, doi:10.1016/j.quascirev.2010.03.010.

Bryan, S. P., T. M. Marchitto, and S. J. Lehman (2010), The release of ¹⁴C-depleted carbon from the deep ocean during the last deglaciation: Evidence from the Arabian Sea, *Earth Planet. Sci. Lett.*, 298(1), 244–254.

Burke, A., and L. F. Robinson (2012), The Southern Ocean's role in carbon exchange during the last deglaciation, *Science*, 335(6068), 557–561.

Butzin, M., M. Prange, and G. Lohmann (2005), Radiocarbon simulations for the glacial ocean: The effects of wind stress, Southern Ocean sea ice and Heinrich events, *Earth Planet. Sci. Lett.*, 235(1–2), 45–61, doi:10.1016/j.epsl.2005.03.003.

Cosma, T. N., I. L. Hendy, and A. S. Chang (2008), Chronological constraints on Cordilleran ice sheet glaciomarine sedimentation from core MD02-2496 off Vancouver Island (western Canada), *Quat. Sci. Rev.*, 27(9), 941–955.

Crusius, J., T. Pedersen, S. Kienast, L. Keigwin, and L. Labeyrie (2004), Influence of northwest Pacific productivity on North Pacific Intermediate Water oxygen concentrations during the Bølling-Allerød interval (14.7–12.9 ka), *Geology*, 32(7), 633–636.

Curry, W. B., and D. W. Oppo (2005), Glacial water mass geometry and the distribution of δ13C of ΣCO2 in the western Atlantic Ocean, *Paleoceanography*, 20, PA1017, doi:10.1029/2004PA001021.

De Pol-Holz, R., L. Keigwin, J. Southon, D. Hebbeln, and M. Mohtadi (2010), No signature of abyssal carbon in intermediate waters off Chile during deglaciation, *Nat. Geosci.*, 3(3), 192–195.

DeVries, T., and F. Primeau (2010), An improved method for estimating water-mass ventilation age from radiocarbon data, *Earth Planet. Sci. Lett.*, 295(3), 367–378.

Duplessy, J.-C., N. J. Shackleton, R. G. Fairbanks, L. Labeyrie, D. Oppo, and N. Kallel (1988), Deepwater source variations during the last climatic cycle and their impact on the global deepwater circulation, *Paleoceanography*, 3, 343–360, doi:10.1029/PA003i003p00343.

Franke, J., A. Paul, and M. Schulz (2008), Modeling variations of marine reservoir ages during the last 45 000 years, *Clim. Past Discuss.*, 4(1), 81–110, doi:10.5194/cpd-4-81-2008.

Galbraith, E. D., S. L. Jaccard, T. F. Pedersen, D. M. Sigman, G. H. Haug, M. Cook, J. R. Southon, and R. Francois (2007), Carbon dioxide release from the North Pacific abyss during the last deglaciation, *Nature*, 449(7164), 890–893, doi:10.1038/nature06227.

Gebbie, G., and P. Huybers (2010), Total matrix intercomparison: A method for determining the geometry of water-mass pathways, *J. Phys. Oceanogr.*, 40(8), 1710–1728.

Gebbie, G., and P. Huybers (2012), The mean age of ocean waters inferred from radiocarbon observations: Sensitivity to surface sources and accounting for mixing histories, *J. Phys. Oceanogr.*, 42, 291–305.

Gorbarenko S. A., I. A. Basov, M. P. Chekhovskaya, J. Southon, T. A. Khusid, and A. V. Artemova (2005), Orbital and millennium scale environmental changes in the southern Bering Sea during the last glacial-Holocene: Geochemical and paleontological evidence, *Deep Sea Res. Part II : Topical Studies in Oceanogr.*, 52(16), 2174–2185.

Gooday, A. J. (2002), Biological responses to seasonally varying fluxes of organic matter to the ocean floor: A review, *J. Oceanogr.*, 58(2), 305–332.

Hain, M. P., D. M. Sigman, and G. H. Haug (2010), Carbon dioxide effects of Antarctic stratification, North Atlantic Intermediate Water formation, and subantarctic nutrient drawdown during the last ice age: Diagnosis and synthesis in a geochemical box model, *Global Biogeochem. Cycles*, 24, GB4023, doi:10.1029/2010GB003790.

Haine, T. W. N., and T. M. Hall (2002), A generalized transport theory: Water-mass composition and age, *J. Phys. Oceanogr.*, 32(6), 1932–1946.

Herguera, J. C., W. H. Berger, and E. Jansen (1992), Evidence for a bathyal front at 2000 m depth in the glacial Pacific, based on a depth transect on Ontong Java Plateau, *Paleoceanography*, 7, 273–288, doi:10.1029/92PA00869.

Horikawa, K., Y. Asahara, K. Yamamoto, and Y. Okazaki (2010), Intermediate water formation in the Bering Sea during glacial periods: Evidence from neodymium isotope ratios, *Geology*, 38(5), 435–438, doi:10.1130/G30225.1.

Hughen, K. A., J. R. Southon, S. Lehman, and J. Overpeck (2000), Synchronous radiocarbon and climate shifts during the last deglaciation, *Science*, 290, 1054–1951.

Ikehara, K., T. Danhara, T. Yamashita, M. Tanahashi, S. Morita, and K. Ohkushi (2011), Paleoceanographic control on a large marine reservoir effect offshore of Tokai, south of Japan, NW Pacific, during the last glacial maximum-deglaciation, *Quat. Int.*, 246(1), 213–221.

Jaccard, S. L., and E. D. Galbraith (2013), Direct ventilation of the North Pacific did not reach the deep ocean during the last deglaciation, *Geophys. Res. Lett.*, 40, 199–203, doi:10.1029/2012GL054118.

Keigwin, L. D. (1998), Glacial-age hydrography of the far Northwest Pacific Ocean, *Paleoceanography*, *13*, 323–339, doi:10.1029/98PA00874.

Keigwin, L. D. (2002), Late Pleistocene-Holocene paleoceanography and ventilation of the Gulf of California, *J. Oceanogr.*, *58*, 421–432.

Keigwin, L. D. (2004), Radiocarbon and stable isotope constraints on last glacial maximum and Younger Dryas ventilation in the Western North Atlantic, *Paleoceanography*, *19*, PA4012, doi:10.1029/2004PA001029.

Key, R. M., P. D. Quay, P. Schlosser, A. P. McNichol, K. F. von Reden, R. J. Schneider, K. L. Elder, M. Stuiver, and H. G. Östlund (2002), WOCE radiocarbon IV: Pacific Ocean results; P10, P13N, P14C, P18, P19, S4P, *Radiocarbon*, *44*(1), 239–392.

Key, R. M., A. Kozyr, C. L. Sabine, K. Lee, R. Wanninkhof, J. L. Bullister, R. A. Feely, F. J. Millero, C. Mordy, and T.-H. Peng (2004), A global ocean carbon climatology: Results from Global Data Analysis Project (GLODAP), *Global Biogeochem. Cycles*, *18*, GB4031, doi:10.1029/2004GB002247.

Kohfeld, K. E., and Z. Chase (2011), Controls on deglacial changes in biogenic fluxes in the North Pacific Ocean, *Quat. Sci. Rev.*, *30*, 3350–3363, doi:10.1016/j.quascirev.2011.08.007.

Kovanen, D., and D. Easterbrook (2002), Paleodeviations of radiocarbon marine reservoir values for the northeast Pacific, *Geology*, *30*(3), 243–246, doi:10.1130/0091-7613(2002)030<0243.

Kuzmin, Y. V., G. S. Burr, and A. J. Timothy Jull (2001), Radiocarbon reservoir correction ages in the Peter the Great Gulf, Sea of Japan, and eastern coast of the Kunashir, Southern Kuriles (Northwestern Pacific), *Radiocarbon*, *43*(2), 477–482.

Kuzmin, Y. V., G. S. Burr, S. V. Gorbunov, V. A. Rakov, and N. G. Razjigaeva (2007), A tale of two seas: Reservoir age correction values (*R*, Δ*R*) for the Sakhalin Island (Sea of Japan and Okhotsk Sea), *Nucl. Instrum. Methods Phys. Res. Sect. B Beam Interact. with Mater. Atoms*, *259*(1), 460–462.

Lund, D. C. (2013), Deep Pacific ventilation ages during the last deglaciation: Evaluating the influence of diffusive mixing and source region reservoir age, *Earth Planet. Sci. Lett.*, *381*, 52–62.

Lund, D. C., A. C. Mix, and J. Southon (2011), Increased ventilation age of the deep northeast Pacific Ocean during the last deglaciation, *Nat. Geosci.*, *4*(11), 771–774, doi:10.1038/ngeo1272.

Lynch-Stieglitz, J., et al. (2007), Atlantic meridional overturning circulation during the Last Glacial Maximum, *Science, 316*(5821), 66–69.

Marchitto, T. M., S. J. Lehman, J. D. Ortiz, J. Flückiger, and A. van Geen (2007), Marine radiocarbon evidence for the mechanism of deglacial atmospheric CO_2 rise, *Science*, *316*, 1456–1459.

Matsumoto, K. (2007), Radiocarbon-based circulation age of the world oceans, *J. Geophys. Res.*, *112*, C09004, doi:10.1029/2007JC004095.

Matsumoto, K., T. Oba, J. Lynch-Stieglitz, and H. Yamamoto (2002), Interior hydrography and circulation of the glacial Pacific Ocean, *Quat. Sci. Rev.*, *21*, 1693–1704.

McNeely, R.. (2006), Geological Survey of Canada, Current Research (Online) no. 2006-G, Natural Resources Canada.

Mekik, F. (2014), Radiocarbon dating of planktonic foraminifer shells: A cautionary tale, *Paleoceanography*, *29*, 13–29, doi:10.1002/2013PA002532.

Mikolajewicz, U., T. J. Crowley, A. Schiller, and R. Voss (1997), Modelling teleconnections between the North Atlantic and North Pacific during the Younger Dryas, *Nature*, *387*, 384–387.

Misarti, N., B. P. Finney, J. W. Jordan, H. D. G. Maschner, J. A. Addison, M. D. Shapley, A. Krumhardt, and J. E. Beget (2012), Early retreat of the Alaska Peninsula Glacier Complex and the implications for coastal migrations of First Americans, *Quat. Sci. Rev.*, *48*, 1–6, doi:10.1016/j.quascirev.2012.05.014.

Ohkushi, K., M. Uchida, K. Aoki, M. Yoneda, K. Ikehara, K. Minoshima, H. Kawahata, R. Tada, M. Murayama, and Y. Shibata (2007), Radiocarbon marine reservoir ages in the northwestern Pacific off Hokkaido Island, Japan, during the last deglacial period, *Radiocarbon*, *49*(2), 963–968.

Okazaki, Y., A. Timmermann, L. Menviel, N. Harada, A. Abe-Ouchi, M. O. Chikamoto, A. Mouchet, and H. Asahi (2010), Deepwater formation in the North Pacific during the Last Glacial Termination, *Science*, *329*(5988), 200–4, doi:10.1126/science.1190612.

Okazaki, Y., K. Kimoto, H. Asahi, M. Sato, Y. Nakamura, and N. Harada (2014), Glacial to deglacial ventilation and productivity changes in the southern Okhotsk Sea, *Palaeogeogr. Palaeoclimatol. Palaeoecol.*, *395*, 53–66.

Oxburgh, R., and W. S. Broecker (1993), Pacific carbonate dissolution revisited, *Palaeogeogr. Palaeoclimatol. Palaeoecol.*, *103*, 31–39.

Rae, J. W. B., M. Sarnthein, G. L. Foster, A. Ridgwell, P. M. Grootes, and T. Elliott (2014), Deep water formation in the North Pacific and deglacial CO_2 rise, *Paleoceanography*, *29*, 645–667, doi:10.1002/2013PA002570.

Reimer, P. J., and R. W. Reimer (2001), A marine reservoir correction database and on-line interface, *Radiocarbon*, *43*(2A), 461–463.

Reimer, P. J., et al. (2013), IntCal13 and Marine13 radiocarbon age calibration curves 0–50,000 years cal BP, *Radiocarbon*, *55*(4), 1869–1887.

Ritz, S. P., T. F. Stocker, and S. A. Müller (2008), Modeling the effect of abrupt ocean circulation change on marine reservoir age, *Earth Planet. Sci. Lett.*, *268*(1–2), 202–211, doi:10.1016/j.epsl.2008.01.024.

Robinson, L. F., and T. van de Flierdt (2009), Southern Ocean evidence for reduced export of North Atlantic Deep Water during Heinrich event 1, *Geology*, *37*(3), 195–198.

Robinson, L. F., J. F. Adkins, L. D. Keigwin, J. Southon, D. P. Fernandez, S.-L. Wang, and D. Scheirer (2005), Radiocarbon variability in the Western North Atlantic during the last deglaciation, *Science*, *310*(5753), 1469–1473.

Robinson, S. W., and G. Thompson (1981), Radiocarbon corrections for marine shell dates with application to southern Pacific Northwest Coast prehistory, *Syesis*, *14*, 45–57.

Sarnthein, M., P. M. Grootes, J. P. Kennett, and M. J. Nadeau (2007), ^{14}C reservoir ages show deglacial changes in ocean currents and carbon cycle, in *Ocean Circulation: Mechanisms and Impacts - Past and Future Changes of Meridional Overturning, Geophys. Monogr. Ser.*, vol. 173, edited by A. Schmittner, J. C. H. Chiang, and S. R. Hemming, pp. 175–196, AGU, Washington D. C.

Sikes, E., C. Samson, T. Guilderson, and W. Howard (2000), Old radiocarbon ages in the southwest Pacific Ocean during the last glacial period and deglaciation, *Nature*, *303*, 555–559.

Skinner, L. C., and N. J. Shackleton (2004), Rapid transient changes in northeast Atlantic deep water ventilation age across Termination I, *Paleoceanography*, *19*, PA2005, doi:10.1029/2003PA000983.

Skinner, L. C., S. Fallon, C. Waelbroeck, E. Michel, and S. Barker (2010), Ventilation of the deep Southern Ocean and deglacial CO_2 rise, *Science*, *328*(5982), 1147–1151.

Skinner, L. C., A. E. Scrivner, D. Vance, S. Barker, S. Fallon, and C. Waelbroeck (2013), North Atlantic versus Southern Ocean contributions to a deglacial surge in deep ocean ventilation, *Geology*, *41*(6), 667–670.

Skinner, L. C., C. Waelbroeck, and A. E. Scrivner (2014), Radiocarbon evidence for alternating northern and southern sources of ventilation of the deep Atlantic carbon pool during the last deglaciation, *Proc. Natl. Acad. Sci.*, *111*(15), 5480–5484.

Smith, V. C., R. A. Staff, S. P. E. Blockley, C. Bronk Ramsey, T. Nakagawa, D. F. Mark, K. Takemura, and T. Danhara (2013), Identification and correlation of visible tephras in the Lake Suigetsu SG06 sedimentary archive, Japan: Chronostratigraphic markers for synchronising of east Asian/west Pacific palaeoclimatic records across the last 150 ka, *Quat. Sci. Rev.*, *67*, 121–137.

Smith, W. H. F., and D. T. Sandwell (1997), Global sea floor topography from satellite altimetry and ship depth soundings, *Science*, *277*(5334), 1956–1962.

Stuiver, M., and H. A. Polach (1977), Discussion: Reporting of ^{14}C data, *Radiocarbon*, *19*(3), 355–363.

Stuiver, M., P. D. Quay, and H. G. Ostlund (1983), Abyssal water carbon-14 distribution and the age of the world oceans, *Science*, *219*(4586), 849–851.

Waugh, D. W., T. M. Hall, and T. W. N. Haine (2003), Relationships among tracer ages, *J. Geophys. Res.*, *108*(C5), 3138, doi:10.1029/2002JC001325.

Wunsch, C., and P. Heimbach (2008), How long to oceanic tracer and proxy equilibrium?, *Quat. Sci. Rev.*, *27*(7), 637–651.

Yoneda, M., H. Uno, Y. Shibata, R. Suzuki, Y. Kumamoto, K. Yoshida, T. Sasaki, A. Suzuki, and H. Kawahata (2007), Radiocarbon marine reservoir ages in the western Pacific estimated by pre-bomb molluscan shells, *Nucl. Instrum. Methods Phys. Res. Sect. B Beam Interact. with Mater. Atoms*, *259*(1), 432–437.